

## Future Changes in European Severe Convection Environments in a Regional Climate Model Ensemble

TOMÁŠ PÚČIK,<sup>a,b</sup> PIETER GROENEMEIJER,<sup>a</sup> ANJA T. RÄDLER,<sup>a,c</sup> LARS TIJSSSEN,<sup>a</sup> GRIGORY NIKULIN,<sup>d</sup> ANDREAS F. PREIN,<sup>e,f</sup> ERIK VAN MEIJGAARD,<sup>g</sup> ROWAN FEALY,<sup>h</sup> DANIELA JACOB,<sup>i</sup> AND CLAAS TEICHMANN<sup>i</sup>

<sup>a</sup> *European Severe Storms Laboratory, Weßling, Germany*

<sup>b</sup> *Department of Geography, Masaryk University, Brno, Czech Republic*

<sup>c</sup> *Georisk Department, Munich Re, Munich, Germany*

<sup>d</sup> *Rosby Centre, Swedish Meteorological and Hydrological Institute, Norrköping, Sweden*

<sup>e</sup> *Wegener Centre for Climate and Global Change, University of Graz, Graz, Austria*

<sup>f</sup> *National Center for Atmospheric Research,<sup>j</sup> Boulder, Colorado*

<sup>g</sup> *Royal Netherlands Meteorological Institute, De Bilt, Netherlands*

<sup>h</sup> *National University of Ireland, Maynooth, Ireland*

<sup>i</sup> *Climate Service Center Germany (GERICS), Helmholtz-Zentrum Geesthacht, Geesthacht, Germany*

(Manuscript received 27 October 2016, in final form 17 April 2017)

### ABSTRACT


The occurrence of environmental conditions favorable for severe convective storms was assessed in an ensemble of 14 regional climate models covering Europe and the Mediterranean with a horizontal grid spacing of 0.44°. These conditions included the collocated presence of latent instability and strong deep-layer (surface to 500 hPa) wind shear, which is conducive to the severe and well-organized convective storms. The occurrence of precipitation in the models was used as a proxy for convective initiation. Two climate scenarios (RCP4.5 and RCP8.5) were investigated by comparing two future periods (2021–50 and 2071–2100) to a historical period (1971–2000) for each of these scenarios. The ensemble simulates a robust increase (change larger than twice the ensemble sample standard deviation) in the frequency of occurrence of unstable environments (lifted index  $\leq -2$ ) across central and south-central Europe in the RCP8.5 scenario in the late twenty-first century. This increase coincides with the increase in lower-tropospheric moisture. Smaller, less robust changes were found until midcentury in the RCP8.5 scenario and in the RCP4.5 scenario. Changes in the frequency of situations with strong ( $\geq 15 \text{ m s}^{-1}$ ) deep-layer shear were found to be small and not robust, except across far northern Europe, where a decrease in shear is projected. By the end of the century, the simultaneous occurrence of latent instability, strong deep-layer shear, and model precipitation is simulated to increase by up to 100% across central and eastern Europe in the RCP8.5 and by 30%–50% in the RCP4.5 scenario. Until midcentury, increases in the 10%–25% range are forecast for most regions. A large intermodel variability is present in the ensemble and is primarily due to the uncertainties in the frequency of the occurrence of unstable environments.

## 1. Introduction

The warming projected by climate models across Europe until 2100 will likely be accompanied by changes in extreme precipitation events (Jacob et al. 2014). Some

of these events result from convective storms that can produce other hazards as well, such as large hail, damaging thunderstorm winds, and tornadoes. Although the literature on changes in extreme precipitation events is steadily expanding, only a few studies have focused on these other hazards in Europe.

Modeling studies of convective hazards are hindered by the small scales of downbursts, tornadoes, and hail. Convection-permitting models with horizontal grid lengths smaller than or equal to 5 km can explicitly simulate the storms that produce these hazards with a reasonable level of accuracy (Weisman et al. 1997). They are able to simulate realistic maxima of precipitation produced by these storms (Prein et al. 2013)

 Denotes content that is immediately available upon publication as open access.

<sup>j</sup> The National Center for Atmospheric Research is sponsored by the National Science Foundation.

Corresponding author: Tomáš Púčik, tomas.pucik@essl.org

DOI: 10.1175/JCLI-D-16-0777.1

© 2017 American Meteorological Society. For information regarding reuse of this content and general copyright information, consult the [AMS Copyright Policy \(www.ametsoc.org/PUBSReuseLicenses\)](http://www.ametsoc.org/PUBSReuseLicenses).

and have also been used by a number of authors to model other convective hazards [see Prein et al. (2015) for a review]. For instance, Trapp et al. (2011) and Gensini and Mote (2014) simulated a historical decade by dynamically downscaling a reanalysis dataset, and Gensini and Mote (2015) simulated storms during a decade at the end of the twenty-first century by dynamically downscaling a global climate model. These studies focused on the central and eastern United States and were able to cover a three-month severe weather season only. To determine the frequency of severe weather, they used updraft helicity, a quantity indicative of strong rotating updrafts, as a proxy for severe convective events (Trapp et al. 2007a). In their study of a dynamically downscaled general circulation model (GCM), Gensini and Mote (2015) found substantial increases in convective hazards in the U.S. springtime storm season during the twenty-first century in the CCSM3 global climate model using the SRES A2 emission scenario.

Other studies used coarser models that parameterize deep, moist convection, and employed proxies that represent environmental controls on the convection (Gensini et al. 2014) rather than the simulated properties of explicitly modeled storms. Typical proxies for convective hazards use a multiplicative combination of convective available potential energy (CAPE), which is a measure of latent instability (Normand 1938), and vertical wind shear between the lower and middle troposphere, also called deep-layer shear (DLS; Brooks et al. 2003). The presence of sizable CAPE ensures that convective updrafts, once initiated, can become strong, whereas the vertical wind shear promotes storm organization and longevity and potentially amplifies the updraft (Weisman and Klemp 1982). The notion that the probability of convective hazards universally is a function of latent instability and DLS is supported by (pseudo)radiosonde studies in the United States (Brooks 2009, 2013), Europe (Groenemeijer and van Delden 2007; Brooks 2013; Púčik et al. 2015), and Australia (Allen and Karoly 2014).

A number of recent studies used this proxy approach to study the evolution of storm environments and applied them to an ensemble of models. Trapp et al. (2009) used an ensemble of five global climate models and found a projected increase in the number of days with a product of CAPE and DLS exceeding 10000 over the United States, with the rate of increase dependent on the geographical region. Allen et al. (2014) found an increase in CAPE in eastern Australia in two different models within strongly warming climate scenarios, and concluded that it will lead to more frequent severe storms. Diffenbaugh et al. (2013) and Seeley and Romps (2015) found that a consensus of CMIP5 (Coupled

Model Intercomparison Project phase 5; Taylor et al. 2012) models simulate a substantial increase of CAPE across the United States as well. These Australian and U.S.-focused studies, using a product of CAPE and DLS to define severe storm environment, concluded that DLS should decrease across the respective regions, but that this does not offset the effect of increasing CAPE.

The authors are aware of only two studies that applied the proxy approach to Europe, both of which used only one rather than multiple climate models: namely, Marsh et al. (2009) found slight decreases of CAPE in summer and slight increases in winter across Europe in one GCM, and Sander (2011) found increases in CAPE and convective inhibition (CIN) in a regional climate model (RCM). A rather different approach, however, was taken by Kapsch et al. (2012), who studied the evolution of severe storms by investigating the frequency of hail-prone circulation patterns across Germany until 2050. Furthermore, Mohr et al. (2015) developed a linear logistic model for hail occurrence across Germany that was based on a combination of parameters and circulation patterns classes, in an ensemble of regional climate model simulations. The latter two studies found modest increases of hail events until the mid-twenty-first century, but with large differences between individual model runs.

The lack of results based on multiple models across Europe was the motivation for the present study, in which we investigated how conditions supportive of convective hazards change during the twenty-first century in two climate scenarios (RCP4.5 and RCP8.5; Moss et al. 2010) using 13 realizations from 5 different RCMs, driven by 10 different GCMs. We investigated two future 30-yr periods, in the middle and at the end of the century, and report on the robustness of the results.

In section 2, we introduce the parameters and their relation to convective hazards. In section 3, we discuss the EURO-CORDEX model data that we have used. In section 4, we report on the changes in latent instability in the two climate scenarios and their constituent components. In section 5, we report on the simultaneous occurrence of instability with wind shear and with modeled precipitation. In section 6, we discuss the differences between the individual models and the implications for the robustness of the results. In section 7, we summarize the main findings, compare them with previous results, discuss the limitations of our approach, and make suggestions for further research.

## 2. Convective storm environment parameters

Following Brooks et al. (2003), we used a measure of latent instability and one of wind shear to characterize convective environments. The lifted index (LI)

represents latent instability and is defined as the difference between the temperature at 500 hPa and the temperature of the parcel that ascends moist-adiabatically from the surface to that level (Galway 1956). It is used as an alternative to CAPE, which was not possible to calculate because only 925-, 850-, 700-, and 500-hPa pressure levels were available for the archived model data. Negative values of the lifted index imply the presence of positive parcel buoyancy at 500 hPa and, equivalently, the presence of latent instability (Normand 1938). Kunz (2007) found that the lifted index is among the most skillful predictors of thunderstorms across southwest Germany. For this study, we included a correction for virtual temperature (Doswell and Rasmussen 1994) and allowed for the parcel to be lifted from any of three source layers (925, 850 and 700 hPa). The lowest resulting LI (i.e., most unstable) was then selected. We ensured that the selected layer was always above the local topography (surface) by preventing layers below the topography from being selected. To show how LI is related to CAPE values, we use a database of soundings from Púčik et al. (2015) that contains 16 000 thunderstorm proximity soundings for central Europe. For these soundings, LI values decrease with increasing CAPE, although there is considerable scatter in CAPE values for a particular value of LI (Fig. 1). This is because LI represents the degree of instability at only one tropospheric level, unlike CAPE, which is a vertical integral of instability.

We have chosen to use potential parcel source layers well above the surface instead of from 2 m above ground level to reduce the dependence of the results on the temperature and humidity at that level. This choice was motivated by the following arguments. First, these values result from parameterizations of temperature and humidity profiles between the surface and the lowest model level. The 2-m temperature and humidity are, unlike pressure level data, diagnostic rather than prognostic variables. Second, we found that using 2-m values leads to suspiciously high instability over the Mediterranean Sea in many of the models, which can be traced back to high moisture at 2 m AGL. Even if correct, such shallow layers are likely not representative of the air flowing into convective clouds in a well-mixed boundary layer (Craven et al. 2002). Last, the possibility of instability from elevated layers would be ignored when exclusively using the 2-m parcel. LI values calculated using 2-m data are generally lower than LI calculated from pressure levels. This is not a problem for this study, since we do not aim for finding a “true value of instability” but rather a metric that discriminates environments unstable enough to sustain severe storms from those that are not (Fig. 3).

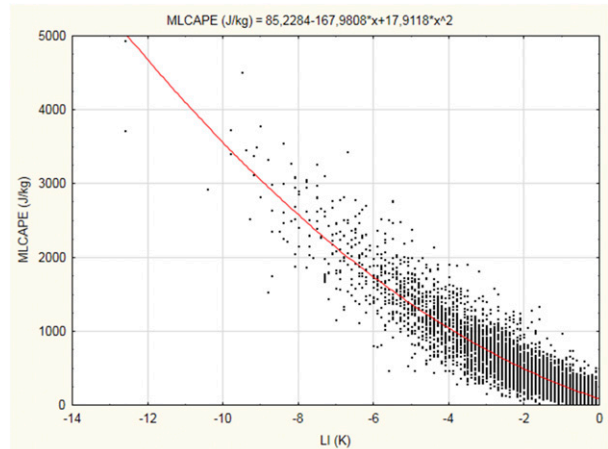


FIG. 1. Scatterplot of LI and CAPE values calculated using a 50-hPa mixed layer based on a database of thunderstorm proximity soundings, described in Púčik et al. (2015). A polynomial regression function was drawn through the data.

Latent instability depends primarily on 1) the moisture content of the source layer of the convection and 2) the lapse rate above it, among other things, such as the lower tropospheric temperature. These two items are two of the three “ingredients” identified for deep, moist convection by Johns and Doswell (1992) and Doswell et al. (1996), the third one being a source of upward motion or lift. Although the parcels we consider can have different source layers, as described above, for simplicity we consider the lapse rate (LARA) or vertical temperature gradient in a fixed layer between the 850 and 500 hPa. Similarly, we use the specific humidity ( $Q$ ) to represent the absolute moisture content of the source layer. These fixed layers will not always be the most representative for the convective conditions in each individual situation. It will be shown in section 4b that these two variables do to a great extent determine LI.

The vertical wind shear is represented by the bulk wind difference between the 500-hPa level and 10 m AGL, and is referred to as deep layer vertical wind shear. The 500-hPa level was chosen instead of an interpolation to, say, 6 km AGL, because such data were not available for all models. Across complex terrain, the 500 hPa to 10-m AGL height difference varies. Thus, across high terrain, where this height difference is smallest, DLS can be expected to be lower in a majority of cases than across low terrain. To illustrate the consequences of the choice, we calculated the relative difference (%) in the number of situations in which with 0–6-km AGL bulk shear and of those in which the 10-m to 500-hPa shear exceeds  $15 \text{ m s}^{-1}$  (a criterion we will be using later). Over most of Europe, the difference is less than 20% (Fig. 2). Across higher terrain mountains, the

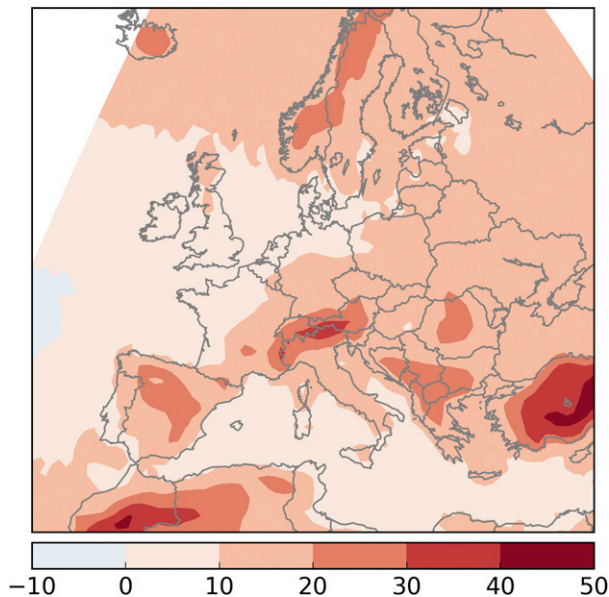


FIG. 2. Relative difference (%) in the number of situations with  $DLS > 15 \text{ m s}^{-1}$  between the calculation using the 6-km AGL height and the calculation using the 500-hPa level in the ERA-Interim dataset for 1981–2000.

difference exceeds 20%. When examining spatial distributions of severe weather environment occurrence, this effect must be kept in mind.

To demonstrate the dependence of convective hazards to both LI and DLS, we investigated the probability of these hazards using ERA-Interim data from 2008 to 2013 (Dee et al. 2011). We followed the procedure employed by Westermayer et al. (2016), whereby reports from the European Severe Weather Database (ESWD; Groenemeijer and Kühne 2014) were matched to LI and DLS values computed at ERA-Interim grid points. A slight modification of Westermayer et al. (2016) was employed such that, for a match, we allowed a severe weather report to occur up to 6 h after an ERA-Interim time step and that we used a slightly different domain (spanning  $6.0$  to  $16.5^\circ$  in longitude and  $45.75$  to  $54^\circ$  in latitude). We considered reports of large hail  $\geq 2 \text{ cm}$ , wind gusts  $\geq 25 \text{ m s}^{-1}$ , and tornadoes, in accordance with the ESWD reporting criteria (Dotzek et al 2009). LI and DLS values of the closest grid point to the report were taken into consideration. In total, 4330 grid points were associated with severe weather, out of total number of 1 578 240 grid points. The ratio of severe to nonsevere grid points in each box increases strongly with decreasing LI and increasing DLS (Fig. 3).

The majority of severe weather events occurs with negative LI, and for all values of LI an increase of DLS is associated with an increase in the ratio of severe grid

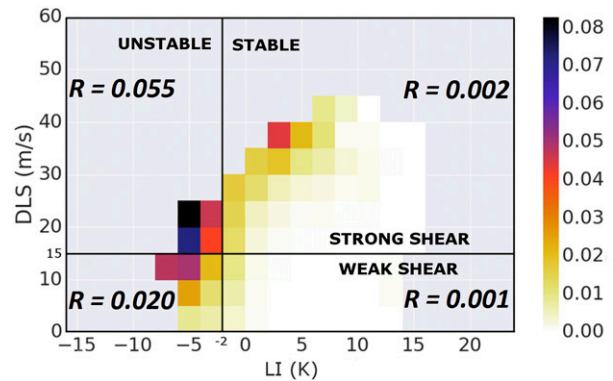


FIG. 3. Ratio ( $R$ ) of the number of grid points associated with severe convective hazard events (hail  $\geq 2 \text{ cm}$ , severe wind gusts  $\geq 25 \text{ m s}^{-1}$ , tornadoes) to nonsevere grid points in the lifted index (LI) and deep-layer shear (DLS) parameter space across central Europe. The labels unstable, stable, weak shear, and strong shear denote subsections of parameter space referred to in the text creating four quadrants. The displayed  $R$  values are the averages of each respective quadrant, rounded to the third decimal place. Boxes representing fewer than 486 grid points are not plotted.

points in each box. Severe weather occurring with positive LI is confined to high-shear environments. In those cases, which typically occur during winter, the convecting layer may not reach up to 500 hPa and the latent instability may not be reflected in a negative LI. Alternatively, the zone of instability may be too narrow and fast-moving to be sampled by the proximity criterion or even by ERA-Interim. The values of the severe weather ratio that we found almost certainly underestimate true probabilities as a result of underreporting in the ESWD (Groenemeijer and Kühne 2014), but this does not prevent us from conducting an analysis of spatial and temporal differences and trends in a relative sense. We have divided the LI and DLS parameter space into quadrants using thresholds (Fig. 3) in order to investigate environments that are the most conducive to severe weather occurrence. In the study, we call an environment for which  $LI \leq -2 \text{ K}$  an *unstable environment*. Whenever  $DLS \geq 15 \text{ m s}^{-1}$ , we call the environment *strongly sheared*. For the quadrant with  $LI \leq -2 \text{ K}$  and  $DLS \geq 15 \text{ m s}^{-1}$ , which represents unstable and strongly sheared environment, the mean ratio is 0.055, much higher than of any other quadrants.

### 3. EURO-CORDEX data

The present study is based on 14 different regional climate models that were run by a number of centers in Europe (Table 1) using a common configuration defined by the EURO-CORDEX initiative (Jacob et al. 2014). EURO-CORDEX is part of the World Climate

TABLE 1. Regional climate model runs used in the study. The scenarios H, 4.5, and 8.5 refer to the historical (1971–2000) control run and the RCP4.5 and RCP8.5 scenarios, respectively. In this study, we refer to the models by the first part of their acronyms (ie. RACMO, RCA). For a list of acronyms used in the table, see the [appendix](#).

Model acronym	Center	RCM	GCM	Member	Scenarios
RACMO-EC-Earth	KNMI	RACMO22E	EC-EARTH	rli1p1	H 4.5 8.5
RACMO-HadGEM			HadGEM2-ES	rli1p1	H 4.5 8.5
RCA-CanESM	SMHI	RCA4	CanESM2	rli1p1	H 4.5 8.5
RCA-CNRM			CNRM-CM5	rli1p1	H 4.5 8.5
RCA-CSIRO			CSIRO-Mk-3.6.0	rli1p1	H 4.5 8.5
RCA-EC-Earth			EC-EARTH	r2i1p1	H 4.5 8.5
RCA-GFDL			GFDL-ESM2M	rli1p1	H 4.5 8.5
RCA-IPSL			IPSL-CM5A-MR	rli1p1	H 4.5 8.5
RCA-MIROC			MIROC5	rli1p1	H 4.5 8.5
RCA-MPI			MPI-ESM-LR	rli1p1	H 4.5 8.5
RCA-NorESM			NorESM1-M	rli1p1	H 4.5 8.5
REMO-MPI			MPI-ESM-LR	rli1p1	H 4.5 8.5
CCLM-HadGEM	MPI-CSC	REMO2009	MPI-ESM-LR	rli1p1	H 4.5 8.5
	CLMCOM	CCLM4	HadGEM2-ES	rli1p1	H 4.5
WRF-EC-Earth	NUIM	WRF341	EC-EARTH	rli1p1	H 8.5

Research Program Coordinated Regional Downscaling Experiment (CORDEX; [Giorgi et al. 2009](#)). The downscaled EURO-CORDEX climate simulations for Europe have horizontal grid spacings of  $0.44^\circ$  ( $\sim 50$  km) and  $0.11^\circ$  ( $\sim 12.5$  km) and cover almost all of Europe, the Mediterranean, and parts of the Atlantic Ocean and North Africa ([Fig. 4](#)). For this study, we only used integrations with a  $0.44^\circ$  grid spacing. More details on EURO-CORDEX model standards can be found in Table 1 in [Kotlarski et al. \(2014\)](#).

Three periods were investigated: a control (historical) run encompassing the 1971–2000 period and the middle (2021–50) and end of the twenty-first-century period (2071–2100). For these future periods, two representative concentration pathway scenarios ([Moss et al. 2010](#)) were assessed (i.e., RCP4.5 and RCP8.5). The RCP2.6 scenario was omitted because too few simulations of these scenarios were available. For four RCMs, runs driven by ERA-Interim reanalysis data were also available: RCA (1981–2010), RACMO (1979–2013), WRF (1989–2010), and CCLM (1989–2009).

The parameters LI, DLS,  $Q$ , and LARA were calculated from two-dimensional fields extracted from the data of the 14 climate models at 6-hourly intervals (i.e., at 0000, 0600, 1200, and 1800 UTC). This was done for the historical run and for both future periods in both climate scenarios. Future changes were addressed by comparing the RCP4.5 and RCP 8.5 climate scenarios during the middle and end periods of the twenty-first century to the historical period. For each investigated parameter, the mean change of individual climate models as well as the sample standard deviation was computed. We classify a change as *robust* whenever it exceeds twice the sample standard deviation, similar to [Diffenbaugh et al. \(2013\)](#).

#### 4. Latent instability and its components

##### a. Lifted index

[Figure 5a](#) shows the ensemble mean of the annual number of unstable environments (i.e.,  $LI \leq -2$  as defined in [section 2](#)) in the historical period and in four future scenarios. In the historical 1971–2000 period, the

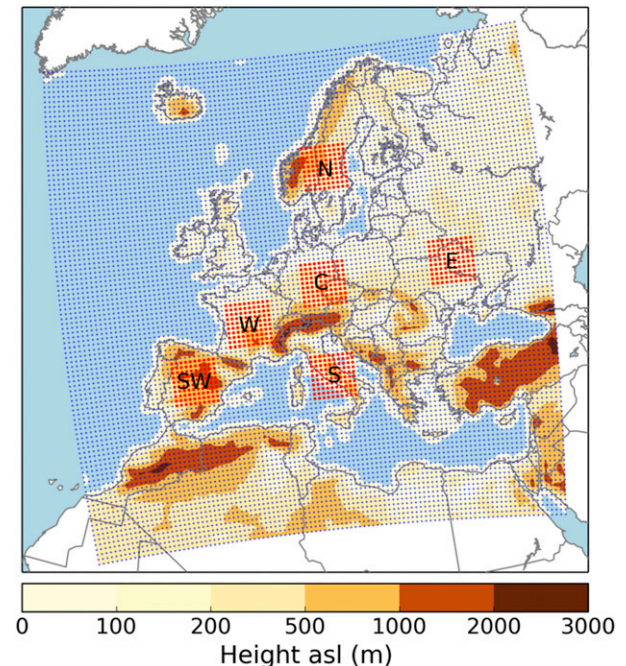


FIG. 4. EURO-CORDEX model domain, individual grid points are represented by blue dots. Model orography (height above sea level) is shown by color scale. Red dots represent the subdomains used below (SW: southwestern Europe, W: western Europe, S: southern Europe, C: central Europe, N: northern Europe, E: eastern Europe).

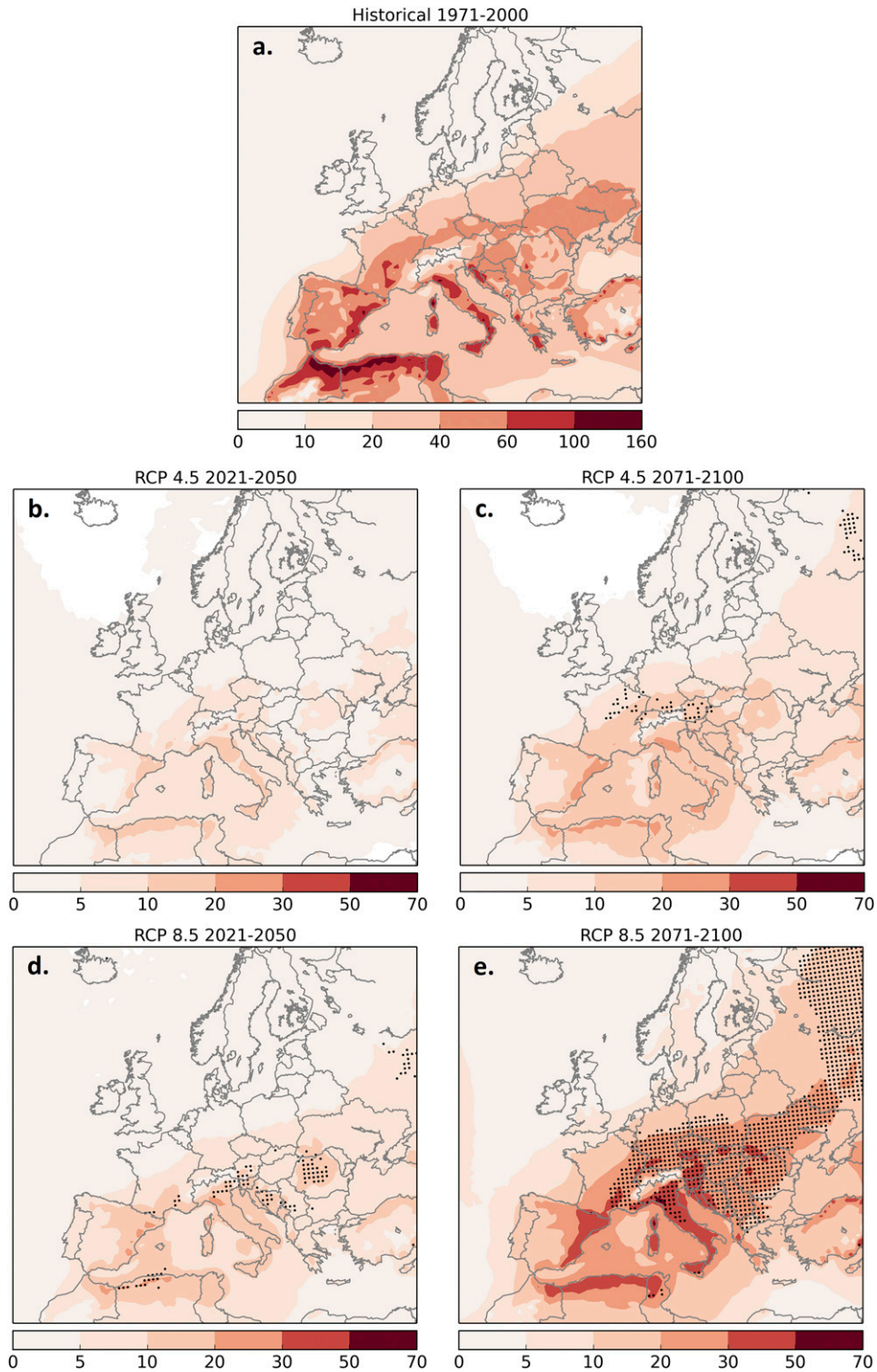


FIG. 5. Ensemble mean value of annual number of unstable environments for (a) the historical 1971–2000 period, and the mean change in the number of environments between the future and historical period for the periods (b) 2021–50 and (c) 2071–2100 in the RCP4.5 scenario, and (d) 2021–50 and (e) 2071–2100 in the RCP8.5 scenario. Black dots are plotted where the ensemble mean change with respect to the historical period exceeds twice the standard deviation of the ensemble spread.

highest values are found along the coastlines of the western Mediterranean Sea with up to 160 occurrences per year. A zone of relatively high number of environments (40–60) stretches from Spain across France and Germany to the Ukraine, while a local minimum is simulated over the Alps.

All future simulations show an increase in the number of unstable environments. The increase is especially pronounced in the RCP8.5 scenario by the end of twenty-first century (Fig. 5e). In that scenario, most of south-central Europe and parts of eastern Europe see a robust increase, with the largest changes projected over the western Mediterranean coastlines and the pre-Alpine areas with an increase of up to 70 environments per year.

By midcentury, the RCP8.5 scenario shows robust changes only near the Mediterranean coastlines and across parts of southeastern Europe (Fig. 5d). The change in the ensemble mean is about half that of the late twenty-first century. For the RCP4.5 scenario (Figs. 5b,c), the changes are smaller and less robust. By the end of the century, significant changes are simulated across parts of central Europe with an increase between 5 to 20 unstable environments per year. Several regions do not show robust changes in either of the scenarios or periods, namely parts of western Russia, Spain, the British Isles, and the southern and southeastern Mediterranean. In spite of the substantial increases in the ensemble mean found for Spain, southern Italy, or Russia, the changes in these areas are not robust owing to a larger model spread.

#### b. Lower tropospheric moisture and lapse rates

To find out how the changes of moisture ( $Q$ ) and lapse rates (LARA) affect the changes in the number of unstable environments, we consider the number of occurrences of particular combinations of these parameters (Fig. 6). Figure 5 shows the mean annual frequency of occurrence of a particular  $Q$ -LARA combination per  $0.5 \text{ g kg}^{-1}$  and  $0.5 \text{ K km}^{-1}$  box at a grid point within each of the six subdomains during the historical period (dashed lines). For southwestern Europe (Fig. 6b), the specific humidity at 850 hPa was taken instead of  $Q$ , as the surface pressure within much of the domain is mostly below 925 hPa. The dotted, continuous, and dotted lines indicate the area of parameter space where the LI is below  $-2$  in 10%, 50%, and 90% of all cases, respectively (i.e., the in right-top part where LARA and  $Q$  are high). For all domains, the high values of LARA are simulated most frequently in the presence of low  $Q$  values, and high values of  $Q$  occur most frequently when LARA is moderate (around  $6 \text{ K km}^{-1}$ ). As a result, unstable environments are relatively rare, in contrast to

the U.S. Midwest, where an overlap of high  $Q$  and high LARA is more frequent in the spring and summer (Brooks et al. 2007).

We now compare the end-of-century RCP8.5 scenario, for which the biggest change in the number of unstable environments was simulated, to the historical period. These changes are shown in blue (decrease) and red (increase) in Fig. 6. The ensemble projects decreases in high-LARA ( $6\text{--}8 \text{ K km}^{-1}$ ) and low- to moderate- $Q$  ( $2\text{--}6 \text{ g kg}^{-1}$ ) environments in all the subdomains, as well as an increase in moderate-LARA ( $4.5\text{--}6.5 \text{ K km}^{-1}$ )/high- $Q$  ( $6\text{--}14 \text{ g kg}^{-1}$ ) environments. In the case of southwestern Europe (Fig. 6b), not only moderate-LARA/high- $Q$  environments, but also high-LARA/high- $Q$  environments increase. Across all subdomains, the decrease in steep LARA environments is projected to occur almost completely out of the section of parameter space that is associated with unstable environments ( $\text{LI} \leq -2$ ). Within that section, an increase is projected across all domains. This increase is especially pronounced for abundant  $Q$  and modest LARA. Since the frequency of environments with steep LARA decreases while that of environments with abundant  $Q$  increases, the effect of increasing  $Q$  is responsible for the projected increases in unstable environments.

## 5. Wind shear and precipitation in unstable environments

### a. Wind shear

We next consider changes in strongly sheared environments (defined according to Fig. 3). In the present-day climate, the highest annual number of strongly sheared environments is simulated over the southwestern Mediterranean and western Europe (600 to 800; Fig. 7a). A higher number of environments is found over western Europe than over the adjacent Atlantic Ocean. This is probably so because the 10-m wind is typically weaker over the land than over the sea. Thus, with the same wind speed at midtroposphere, stronger DLS occurs over the land, unless the wind directions have opposite components. The least number of strongly sheared environments is simulated over the northern Atlantic and southeastern Europe (300–500).

Over the course of the century, almost no robust changes in DLS are simulated, except for the northern Atlantic, northern Scandinavia, and northern Russia. Here, the simulated decrease is robust in both scenarios and both investigated future periods. By the end of the century in the RCP8.5 scenario (Fig. 7e), a decrease by up to 120 environments per year is projected over this area. The decrease is caused mainly by the reduction in

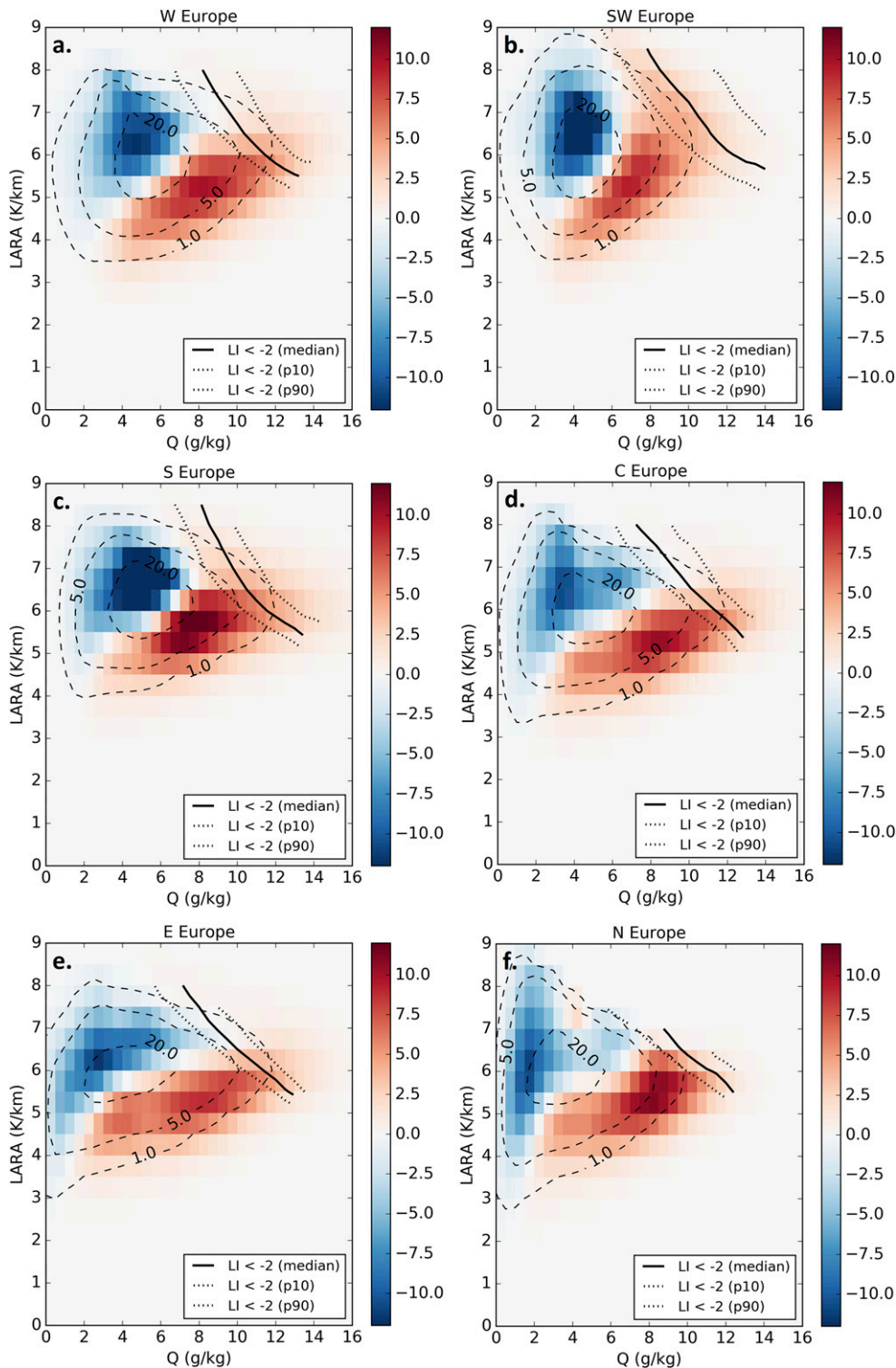


FIG. 6. 2D histograms showing the regionally averaged ensemble mean annual numbers of environments with given range of  $Q$  and LARA values (dashed black contours) and their mean change between the RCP8.5 scenario, 2071–2100 period and the 1971–2000 period (color scale) for (a) western, (b) southwestern, (c) southern, (d) central, (e) eastern, and (f) northern Europe, as defined in Fig. 3. The histogram bins are  $0.5 \text{ g kg}^{-1}$  wide and  $0.5 \text{ K km}^{-1}$  tall. The two dotted and one solid lines represent the 10th, 50th, and 90th percentiles of the  $Q$  and LARA values associated with  $\text{LI} < -2 \text{ K}$ .



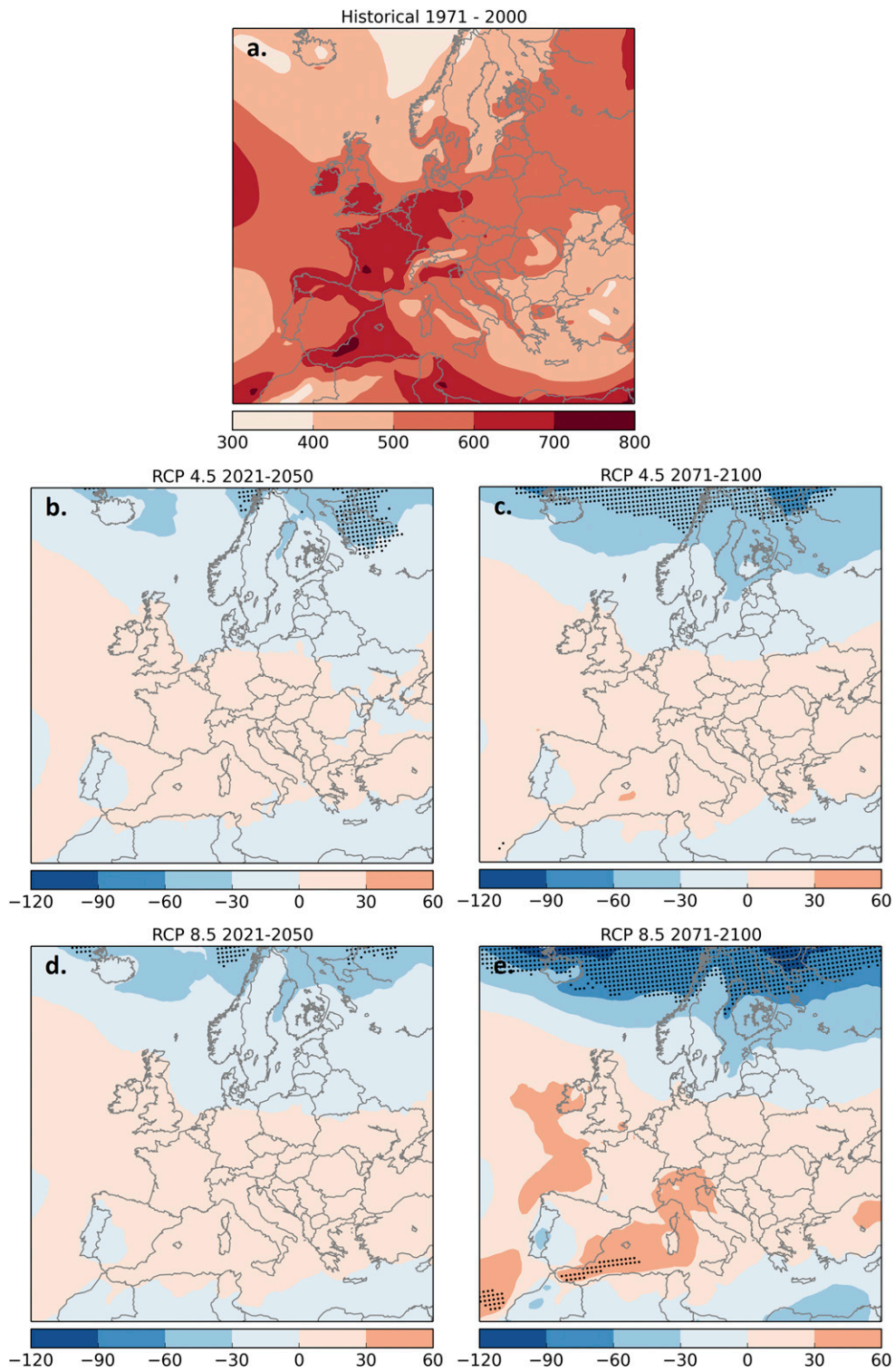


FIG. 7. As in Fig. 4, but for mean annual number of strongly sheared environments.

the 500-hPa flow rather than by changes of the 10-m wind (not shown). However, the strongest decrease is confined to an area that experiences little if any unstable environments (Fig. 4a). A small, but not robust, increase in the number of environments is projected in the belt from western to southeastern Europe in both scenarios and periods. In the RCP8.5 scenario by 2100, a robust increase by up to 60 environments per year is simulated for the southwestern Mediterranean.

### b. Instability and wind shear parameter space

So far we have considered specific thresholds in the LI and DLS parameter space. To investigate changes in the whole parameter space, a similar approach is employed as in Fig. 6 (2D parameter space of  $Q$  and LARA). In the current climate, the most frequently visited region in LI–DLS parameter space is similar for all areas with LI values ranging between 0 and 5 K and DLS values ranging between 3 and 20  $\text{m s}^{-1}$  (Fig. 8, dashed lines). The frequency rapidly decreases for decreasing LI (more unstable environments) across all of the subdomains. For unstable environments, frequency decreases with increasing DLS, thus the majority of unstable environments are weakly sheared ( $\text{DLS} < 15 \text{ m s}^{-1}$ ).

In the future (RCP8.5 scenario and 2071–2100 period), an increase of both unstable and very stable environments ( $\text{LI} > 7 \text{ K}$ ) is projected across all the domains. At the same time, a decrease in the number of slightly stable environments ( $0 < \text{LI} < 5 \text{ K}$ ) is simulated, except for northern Europe. The unstable and strongly sheared environments show an increase in all domains, albeit very small across northern Europe.

There are some differences in the changes in the LI–DLS parameter space among the studied domains. For western, southwestern, and southern Europe (Figs. 8a–c), the increase in the number of unstable environments is the strongest in weakly sheared environments, but it shifts more toward strongly sheared environments in case of eastern and central Europe (Figs. 8d,e). Northern Europe (Fig. 8f) shows the most pronounced future changes in the instability dimension (i.e., toward weakly stable and weakly sheared environments). Note that the domain is still located south of where DLS is projected to decrease (Fig. 7e).

### c. Precipitation in unstable environments

The presence of latent instability does not guarantee that a thunderstorm will form, so that it is not clear whether increases in instability are associated with increases in thunderstorm activity. We may, however, suppose that thunderstorms become much more likely when the model produces precipitation in a given unstable environment, which has been done before by

Trapp et al. (2009). Indeed, a comparison of lightning occurrence with ERA-Interim precipitation and the lifted index shows that, for  $\text{LI} \leq -2$ , the probability of lightning is below 0.05 when the model does not produce any precipitation, but it is much higher in presence of even small amounts of precipitation (Fig. 9). The probability is defined as the relative frequency that more than one lightning strike was detected by the EUCLID network (Schulz et al. 2016) in a  $0.75^\circ \times 0.75^\circ$  model grid box within the 3 h after the time at which the given LI was simulated, and during the 3 h for which the indicated amount of precipitation was simulated. The period comprises the years 2008 through 2013 and the area of study is a region covering a large part of Europe (see Westermayer et al. 2016). We will from now on call any environment with accumulated precipitation  $\geq 1 \text{ mm}$  in 6 h a *precipitating environment*. Precipitating environments that are also unstable ( $\text{LI} \leq -2$ ) will be called *thunderstorm environments*, while we are aware that thunderstorm initiation in such conditions is by no means guaranteed.

In the historical runs, the most frequent occurrence of thunderstorm environments is simulated over the mountains and hills of southern and central Europe and the coasts of the northern Mediterranean (Fig. 10a). A minimum located over the central Alps can be attributed to a minimum of instability and is confirmed by lightning observation data (e.g., Poelman et al. 2016; Anderson and Klugmann 2014). Other observed local maxima across the Gulf of Genoa, Corsica, and around the eastern coast of the Adriatic Sea are reproduced as well. An observed maximum of lightning frequency over northeastern Italy (e.g., Anderson and Klugmann 2014, their Fig. 4) is not reproduced in the EURO-CORDEX  $0.44^\circ$  models used in this study (Fig. 10a).

During the twenty-first century, the consensus of the ensemble indicates an increase in thunderstorm environments over most of Europe, with the strongest and most significant change associated with the RCP8.5 scenario in the 2071–2100 period (Fig. 10e). The increase is smaller in the RCP4.5 scenario and the 2021–51 period (Figs. 10b–d). The largest increase is projected to occur over south-central and central Europe. A robust increase is simulated across parts of central and eastern Europe.

The changes in frequency of thunderstorm environments do not completely correspond with that of instability (Fig. 5). The area where robust signals are detected is smaller and the rate of increase is less pronounced over southern Europe, especially the southern Mediterranean coastlines. Therefore, the future trends in the precipitating environments must be considered separately to explain the differences.

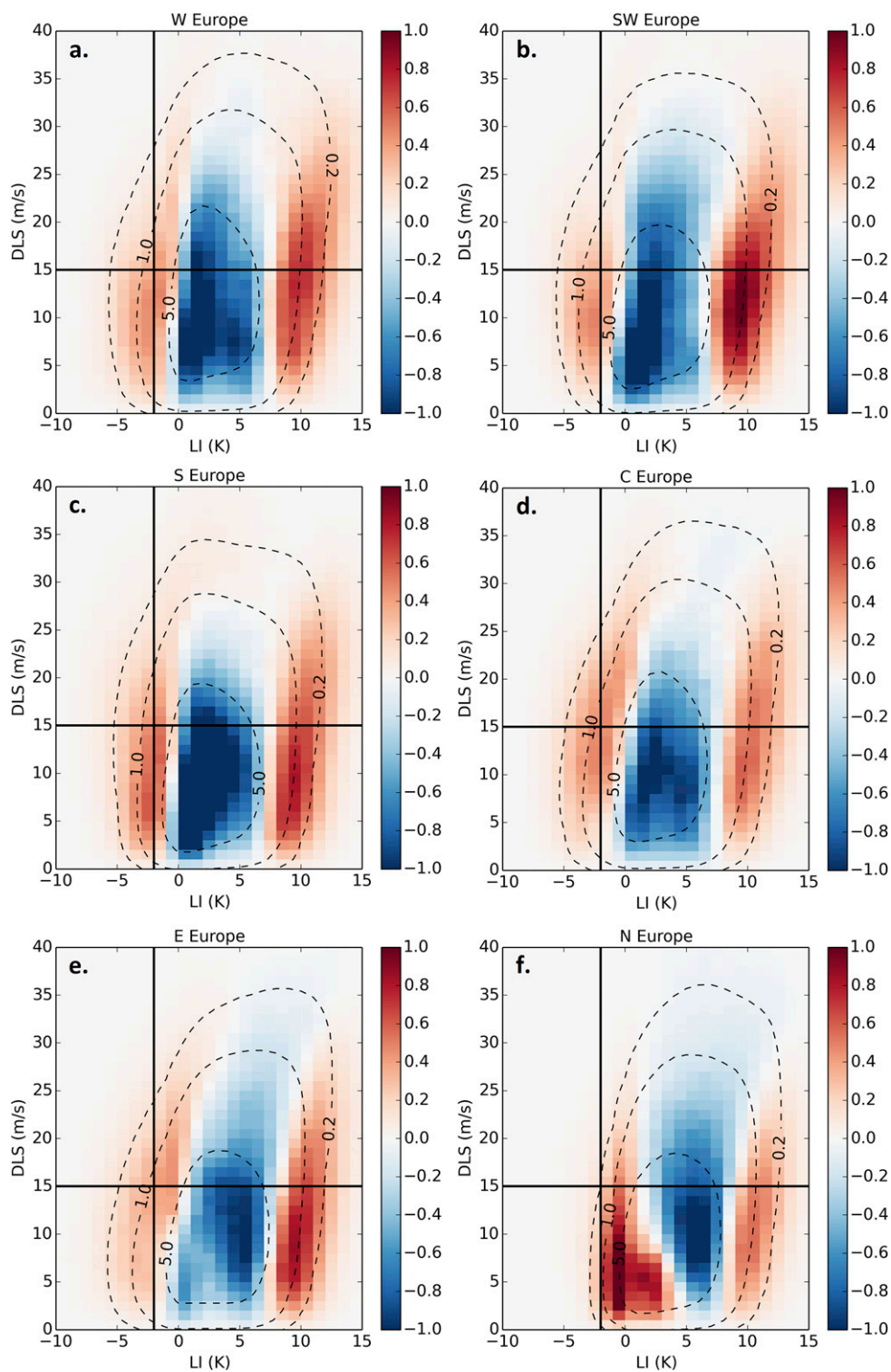


FIG. 8. As in Fig. 5, but for the LI and DLS parameter space and histogram bin dimensions of 1 K and  $1 \text{ m s}^{-1}$  grid space. Thick lines denote the LI and DLS threshold values for unstable and strongly sheared environment as introduced in section 2 and Fig. 2.

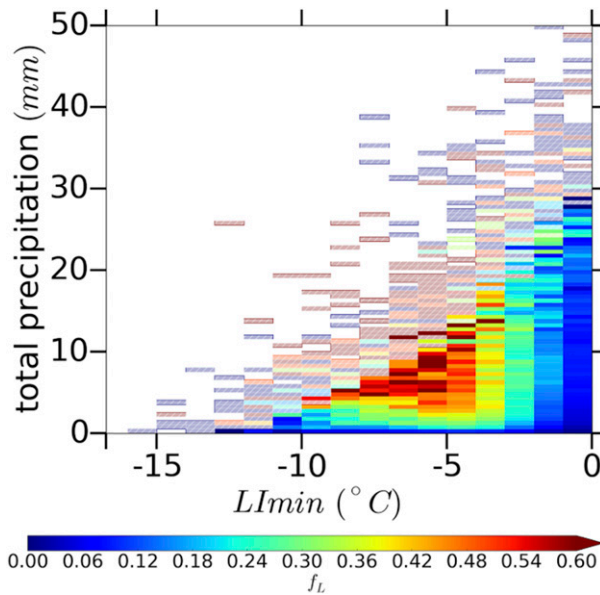


FIG. 9. Relative frequency of lightning as a function of 6-hourly precipitation and LI based on 2008–13 lightning and ERA-Interim data over central Europe. Bins with less than 10 cases are hatched.

Changes in the mean annual number of precipitating environments (Fig. 11b) differ strongly across Europe. Over northern Europe, a robust increase is projected whereas changes in central Europe are insignificant. Across western and southern Europe, the number of events decreases. A strong and robust decrease is simulated over much of southern Europe, especially over Iberia, southern Italy, and the southern Balkans. Although a strong increase in low-level humidity ( $Q$ ; Fig. 6) and unstable environments (Fig. 5) is simulated over southern and southwestern Europe, it will rain less frequently. The smaller number of precipitating environments compensates for the increase in the number of unstable environments, resulting in a smaller change in the number of thunderstorm environments compared to central Europe. The changes in the number of precipitating environments pertain to modeled precipitation, regardless of whether it was or was not convective in nature.

Another way to explain the differences between the changes in the unstable and thunderstorm environments is to consider the “efficiency” with which unstable environments result in precipitation. We define the efficiency as the fraction of the number of unstable environments that were also precipitating. In the historical runs, this fraction (ratio) is the highest over the mountainous areas (locally up to 0.8 over the Alpine range) and is higher over northern than over southern Europe (Fig. 11c). Over the central Alps, the number of unstable environments is too small ( $<10$ ) to compute

the fraction. The lowest values ( $<0.1$ ) are simulated over the coastlines of northern Africa. A future decrease in ratio is projected across all of Europe. The strongest relative decrease is found across eastern Spain, southern France, and parts of northern Africa (Fig. 11d).

#### d. Precipitation in strongly sheared and unstable environments

Because of the increase in instability and little change in the wind shear over large parts of Europe, an increase in severe convective storm environments (unstable and strongly sheared) may be expected. To investigate the spatial and temporal changes of the number of such environments, a similar threshold approach as in section 5c was used. Besides the thresholds for unstable and precipitating environment, a threshold for DLS ( $\geq 15 \text{ m s}^{-1}$ , based on Fig. 3) was implemented to include only the strongly sheared environments. The chosen threshold coincides with the lower bounds of DLS associated with supercells (Rasmussen and Blanchard 1998; Thompson et al. 2003), which are virtually always accompanied by severe convective hazards (Duda and Gallus 2010). We will refer to an unstable, strongly sheared and precipitating environment as a *severe* environment.

In the historical period, local maxima in severe environments are located over southern France, eastern Spain, northwestern Italy, the eastern Adriatic Sea coastline, and northern Africa with over eight events per year (Fig. 12a). The local maxima over eastern Europe are less pronounced when DLS is included as a threshold (cf. Figs. 12a and 10a). This is due to the lower frequency of strongly sheared environments compared to other areas. The frequency of severe environments generally decreases toward the northwest and north.

In the future, an increase in the frequency of severe environments is projected, especially over central and south-central Europe, with an increase by two to eight events per year (up to 100% increase) by the 2071–2100 period in the RCP8.5 scenario (Fig. 12e). For both periods in the RCP4.5 scenario (Figs. 12b,c) and the RCP8.5 scenario 2021–50 period (Fig. 12d) there are almost no grid points displaying a robust change. By the end of the century, the RCP4.5 scenario projects a robust change over small parts of central and eastern Europe. By the same time, for RCP8.5 scenario, a robust increase is found over large portions of continental Europe, in a belt stretching from central Europe and the northern Adriatic Sea toward Russia. A comparable magnitude of increase to central Europe is also simulated for northeastern Spain and central Italy. However, future development is more uncertain here as the mean increase was not deemed robust. In case of the RCP8.5

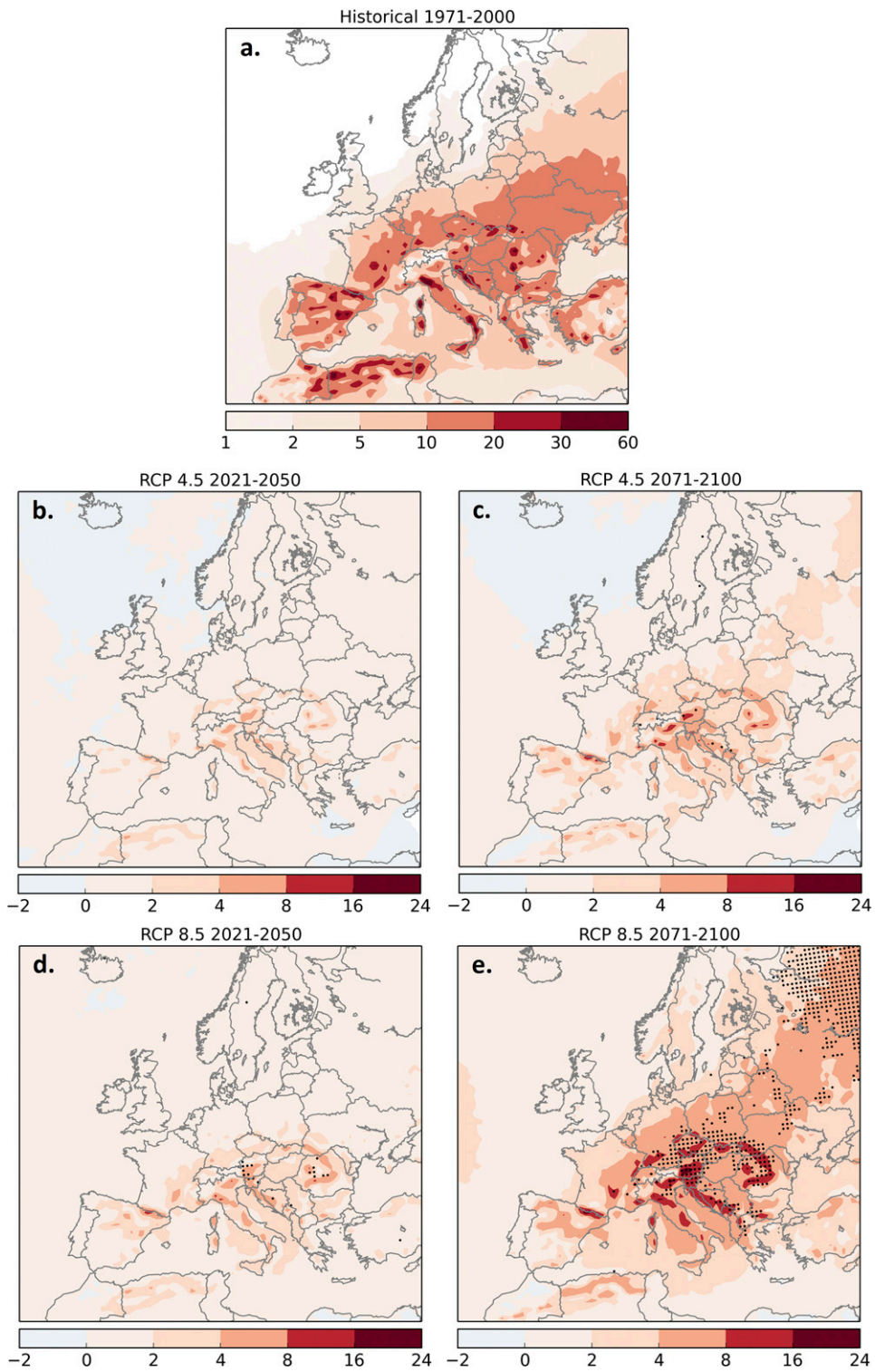


FIG. 10. As in Fig. 4, but for the annual number of unstable and precipitating environments.

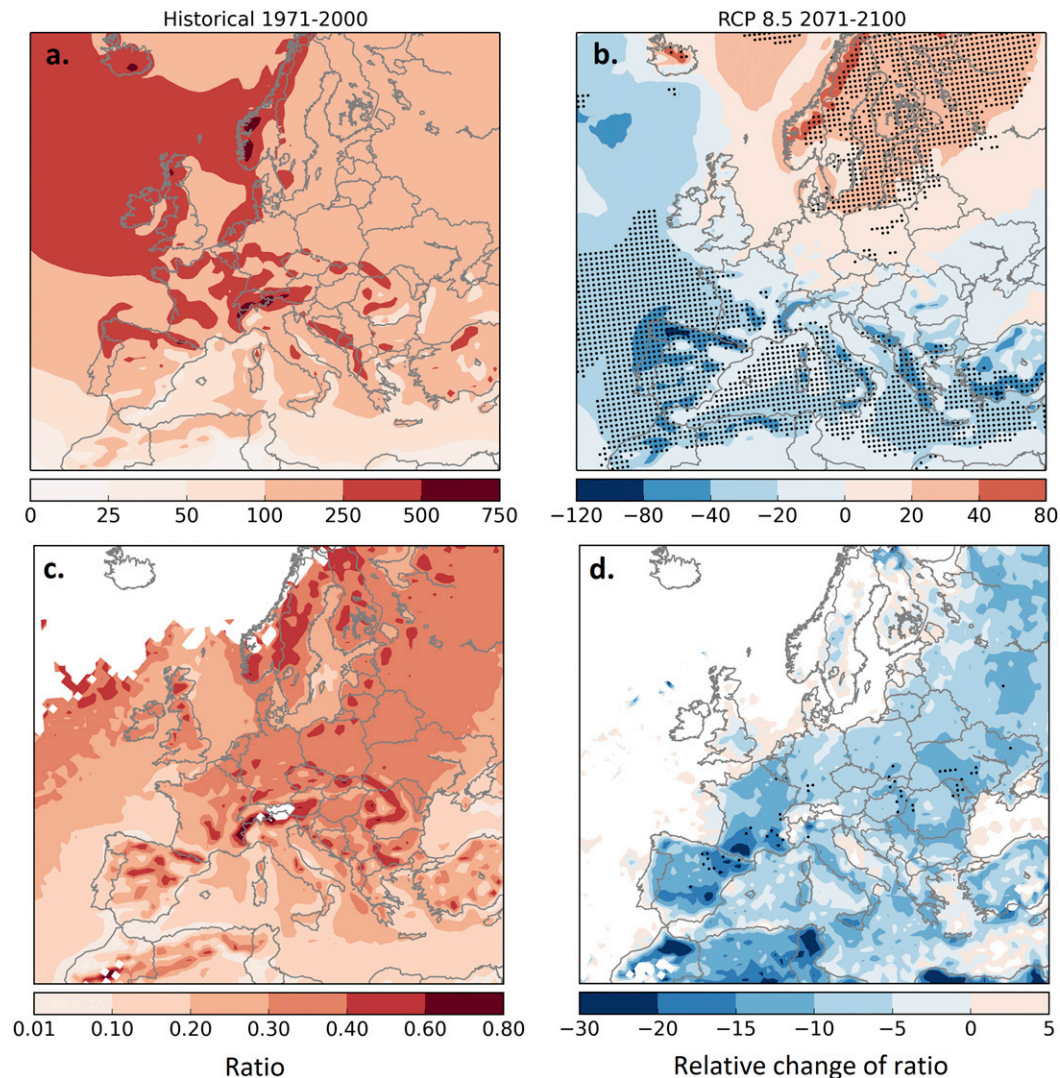


FIG. 11. (a) Mean annual number of precipitating environments in the historical 1971–2000 period. (b) Change in the annual number of precipitating environments between the RCP 8.5 2071–2100 and the historical period. (c) Mean ratio between the unstable and precipitating environments to unstable environments in the historical 1971–2000 period. (d) Relative change (%) in the mean ratio between the RCP 8.5 2071–2100 and the historical period.

scenario and 2071–2100 period, the increase in the number of severe environments is robust over a larger parts of central and eastern Europe than the increase in the number of convective storms (Fig. 10e). The likely reason is that the increase in the unstable environments is shifted more toward the strongly sheared parameter space (Fig. 8).

Seasonally, the highest frequency of severe environments is simulated in the summer (Fig. 13c), with an exception of the central Mediterranean, where the maximum is found either in the autumn or summer (Fig. 13e). A comparatively smaller number of severe environments is simulated for spring and winter

(Figs. 13a,g). In the future (RCP 8.5 scenario and 2071–2100 period), a pronounced increase in the severe environments is projected in spring across much of Europe (Fig. 13b). This increase is notable in relative sense (given the low number of environments in the historical period) with a magnitude of more than 100% over the parts of western, central, and southern Europe. In the summer, there is an increase as well, which is largest across central Europe (Fig. 13d). Very little if any increase is simulated over far western and southwestern Europe, which can be attributed to the decrease of precipitating environments in this season (not shown). In autumn, an increase in severe environments is

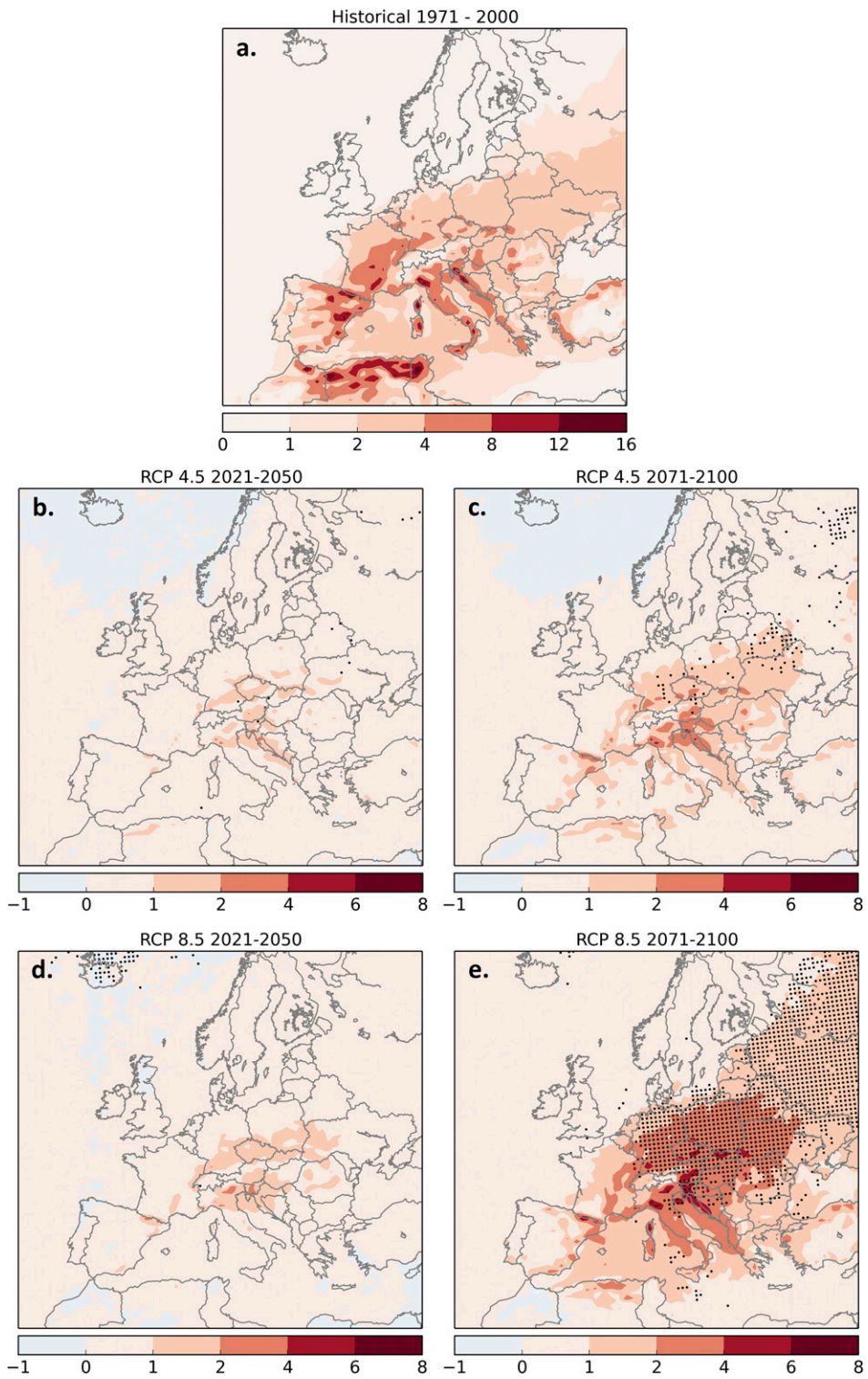


FIG. 12. As in Fig. 4, but for the mean annual number of severe environments.

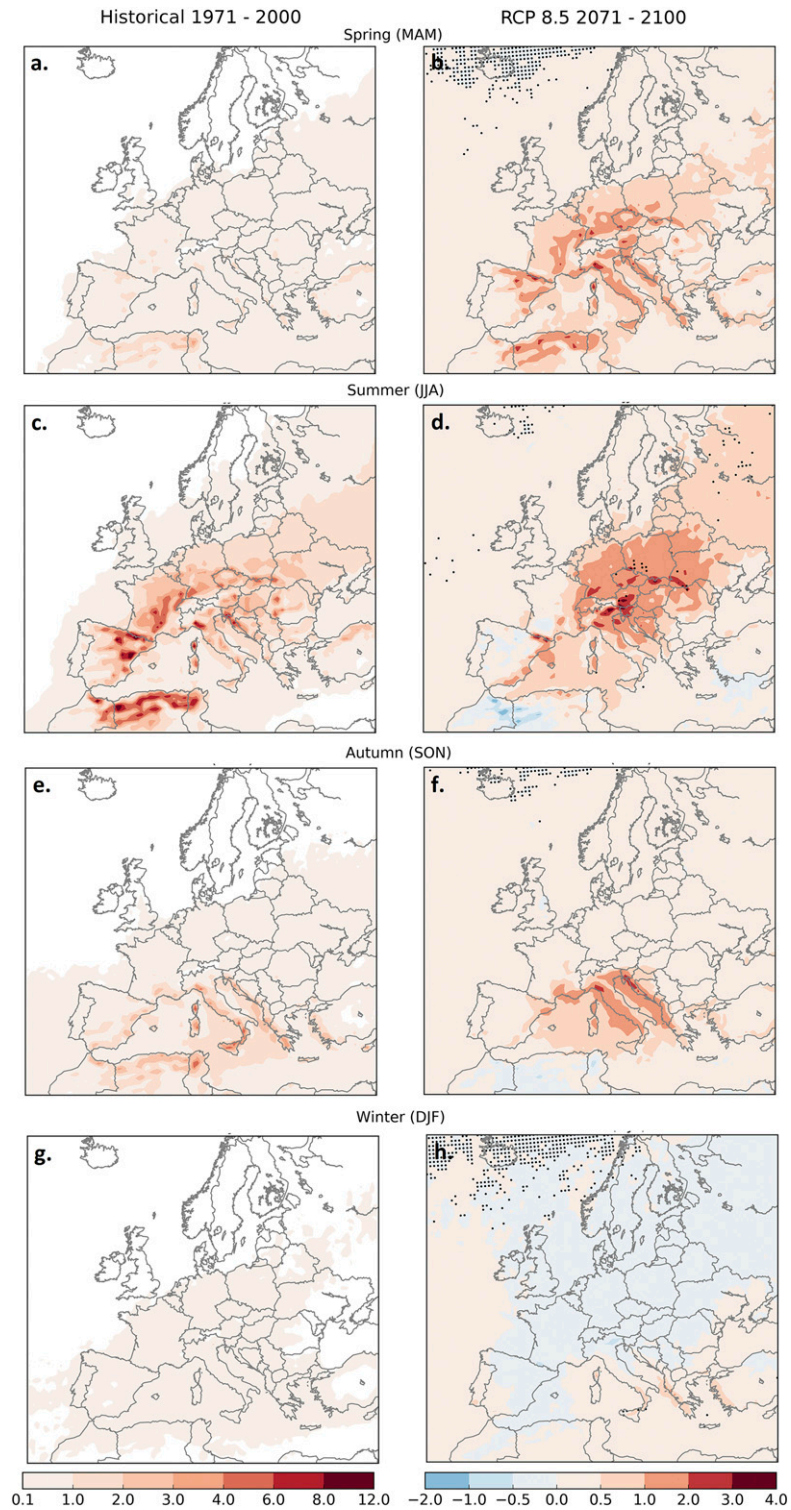


FIG. 13. Mean annual number of severe environments in the historical 1971–2000 period in (a) spring (MAM), (c) summer (JJA), (e) autumn (SON), and (g) winter (DJF) and change in the mean annual number of severe environments between the RCP 8.5 2071–2100 and the historical period in (b) MAM, (d) JJA, (f) SON, and (h) DJF.



predicted across the Mediterranean Sea and its coastlines (Fig. 13f). In the winter, only very small changes are projected everywhere (Fig. 13h). In contrast to the changes aggregated over the whole year (Fig. 12e), only a few grid points show robust changes.

## 6. Comparison of model consensus to reanalysis and intermodel variability

The identification of any model biases is important for the interpretation of the model results. It is beyond the scope of this study to identify biases for each of the used models, but a comparison between the EURO-CORDEX ensemble and ERA-Interim, and a discussion of variability within the model ensemble is in order. The mean annual number of severe environments in the EURO-CORDEX ensemble (Fig. 14a) and ERA-Interim reanalysis (Fig. 14b) in the period 1981–2000 shows similar large scale patterns and have local maxima along the Mediterranean Sea coastlines. The EURO-CORDEX ensemble produces more local variation related to topography, which is due to the better resolution ( $0.44^\circ$  horizontal grid spacing vs  $0.75^\circ$ ) and it has higher number of severe environments than ERA-Interim in most places. The EURO-CORDEX ensemble also has a positive bias of the number of unstable environments, with the exception of southern and southeastern Europe (Figs. 14c,d). The mean annual number of strongly sheared environments shows differences over Scandinavia, where EURO-CORDEX has a negative bias with respect to ERA-Interim (Figs. 14e,f). Regarding precipitating environments, EURO-CORDEX shows a positive bias over the mountains and western Europe, which may also be an effect of the higher resolution of the ensemble.

After we addressed the variability among the RCMs only indirectly by indicating the robustness of changes, we now consider the behavior of individual models. A large spread in the mean annual number of the severe environments is evident for the historical period. There is more than a twofold difference between the least and most “severe” model (Figs. 15a,b). The spread increases in the future period up to an almost threefold difference between the least and most aggressive model in the RCP8.5 scenario in the 2071–2100 period (Fig. 15b). A large spread of comparable magnitude is present in the evaluation runs of RCM models driven by the ERA-Interim reanalyses (Figs. 15a,b). This suggests that the RCMs employed for the downscaling are an important source of intermodel variability. That said, the lowest and highest number of severe grid points in the historical (1971–2000) runs are found in runs of the same RCM (i.e., the RCA model). In this case, the GCMs create

variability. Despite the large spread, all ensemble members agree on future increases in the RCP8.5 scenario. Similarly, in the RCP4.5 scenario, there is an agreement among models regarding the sign of the changes, with the exception of only one ensemble member (CCLM-HadGem).

As with the absolute changes, the individual models also show fair agreement regarding the relative changes. For the RCP4.5 scenario and 2071–2100 period, the relative change in the total number of severe events across the entire domain varies between  $-0.07$  and  $+0.50$ , and for the RCP8.5 scenario and the same period, it varies between  $+0.25$  and  $+0.88$  (Figs. 15c,d). All 13 models that were available for both RCP scenarios are consistent in simulating stronger relative increases in the RCP8.5 than in the RCP4.5 scenario.

By breaking up the criterion of severe into its three conditions of instability, strong shear, and precipitation, the origins of the intermodel variability can be traced back to its components. Unstable environments (Fig. 16a) display the largest model spread, while both strongly sheared (Fig. 16b) and precipitating environments (Fig. 16c) have a much smaller spread. Similar to the number of severe environments (Figs. 15a,b), a more than twofold difference exists between the highest and the lowest value of unstable environments in the historical period (Fig. 16a). Although all models point in the direction of an increase, the rate of increase differs among them.

Strongly sheared and precipitating environments show less intermodel variability and no increase in the future. For strongly sheared environments (Fig. 16b), nine of the ensemble members project a slight decrease in the number of grid points, while the remaining three show a slight increase. For precipitating environments (Fig. 16c), a slight decrease toward the future is simulated by most of the models. For both environments, ERA-Interim-driven model runs show much less spread than in case of the unstable environments. Therefore, the main source of uncertainty and intermodel variability in the simulations is the instability.

## 7. Discussion and conclusions

An increase in frequency of environments supportive of severe convective storms is projected over Europe in the twenty-first century in both RCP scenarios according to 14 regional climate models. The strongest increase is simulated for the RCP8.5 scenario and by the 2071–2100 period, yielding robust changes over most of south-central, central, and eastern Europe. Less robust and smaller increases are simulated for both studied periods of the RCP4.5 scenario and the 2021–50 period of the

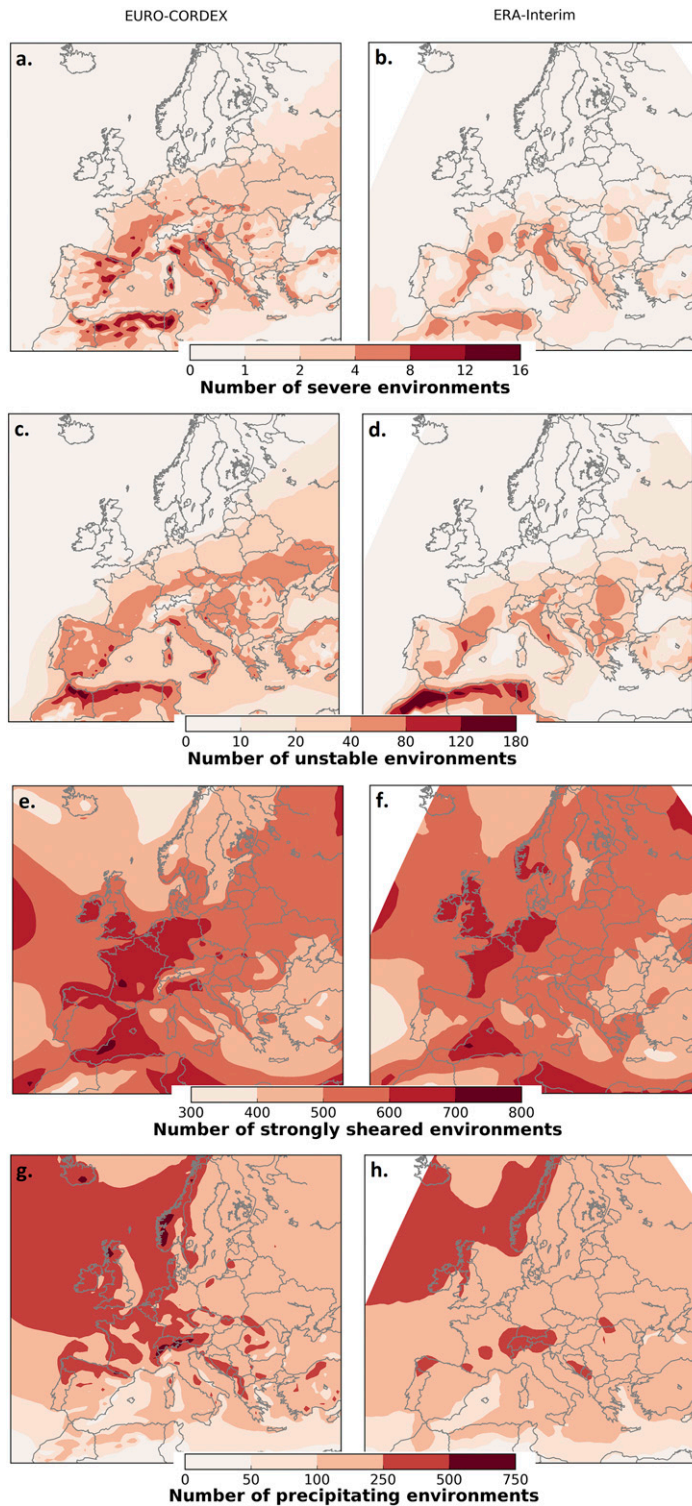


FIG. 14. Mean annual number of (a),(b) severe environments, (c),(d) unstable environments, (e),(f) strongly sheared environments, and (g),(h) precipitating environments in EURO-CORDEX (ensemble average) and in ERA-Interim for the period 1981–2000, respectively.

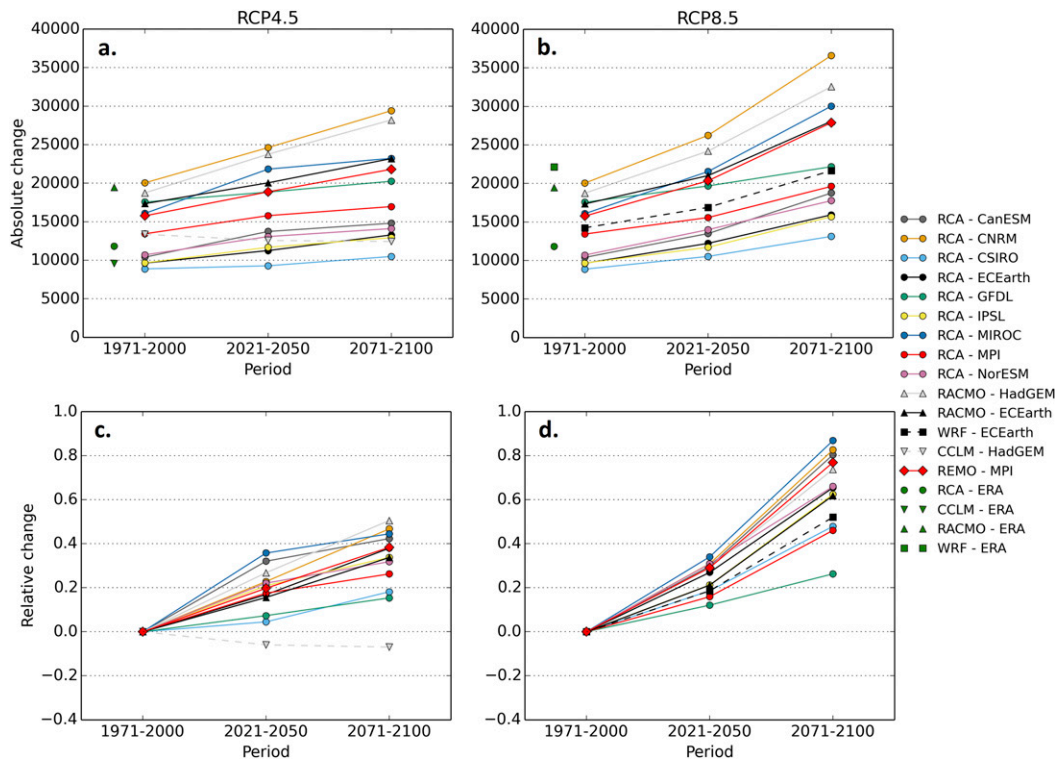


FIG. 15. (a) Mean annual number of severe environments across the whole domain for individual model runs in the 1971–2000, 2021–50, and 2071–2100 periods of the RCP4.5 scenario and for the ERA-Interim driven runs (green symbols). (b) As in (a), but for the RCP8.5 scenario. (c) A relative change in the mean annual number of severe environments between the future (2021–50 and 2071–2100) and the historical (1971–2000) periods of the RCP4.5 scenario. (d) As in (c), but for the RCP8.5 scenario.

RCP8.5 scenario. We do not detect any geographical shifts of the increases changes between the two RCP scenarios or between the two time intervals (i.e., historical to 2021–50, and 2021–50 to 2071–2100): the strongest increases are projected consistently for south-central Europe. The future changes are primarily caused by an increase in latent instability, which results from an increase in the lower tropospheric moisture.

These results are similar to those found in the United States or in Australia, where increases in severe storm environments caused by increased instability have been found as well (Del Genio et al. 2007; Trapp et al. 2007b; Marsh et al. 2009; Trapp et al. 2009; Diffenbaugh et al. 2013; Allen et al. 2014; Seeley and Romps 2015). Like in Europe, the driver for the increase in instability over United States and Australia was found to be higher moisture content in the lower troposphere (Trapp et al. 2007b, 2009; Allen et al. 2014; Seeley and Romps 2015).

In contrast to the United States or Australia, vertical wind shear is projected not to undergo any robust changes during the twenty-first century across Europe, except for northern Scandinavia. The EURO-CORDEX ensemble shows mostly no robust changes

in DLS, whereas a decrease was found across much of the United States (Trapp et al. 2007b, 2009) and Australia (Allen et al. 2014). Although Diffenbaugh et al. (2013) found that the decrease in shear across the United States happens mostly in situations with low instability, the ensemble of EURO-CORDEX simulations presented here shows robust decreases in DLS neither in slightly nor in strongly unstable environments.

In Europe, Kapsch et al. (2012) investigated the effects of frequency changes of synoptic flow patterns to the occurrence of large hail over Germany. The magnitude of the increase in the EURO-CORDEX ensemble is much larger than theirs, which suggests that there are important additional factors beyond the more frequent occurrence of hail-prone circulation patterns, in particular the increase in low-level humidity regardless of the flow pattern.

The intermodel variability in the number of severe convective environments among the EURO-CORDEX models is caused primarily by the differing amounts of instability, for which large differences were noted even in the reanalysis-driven runs. Variability in both the reanalysis-driven and the global climate model driven

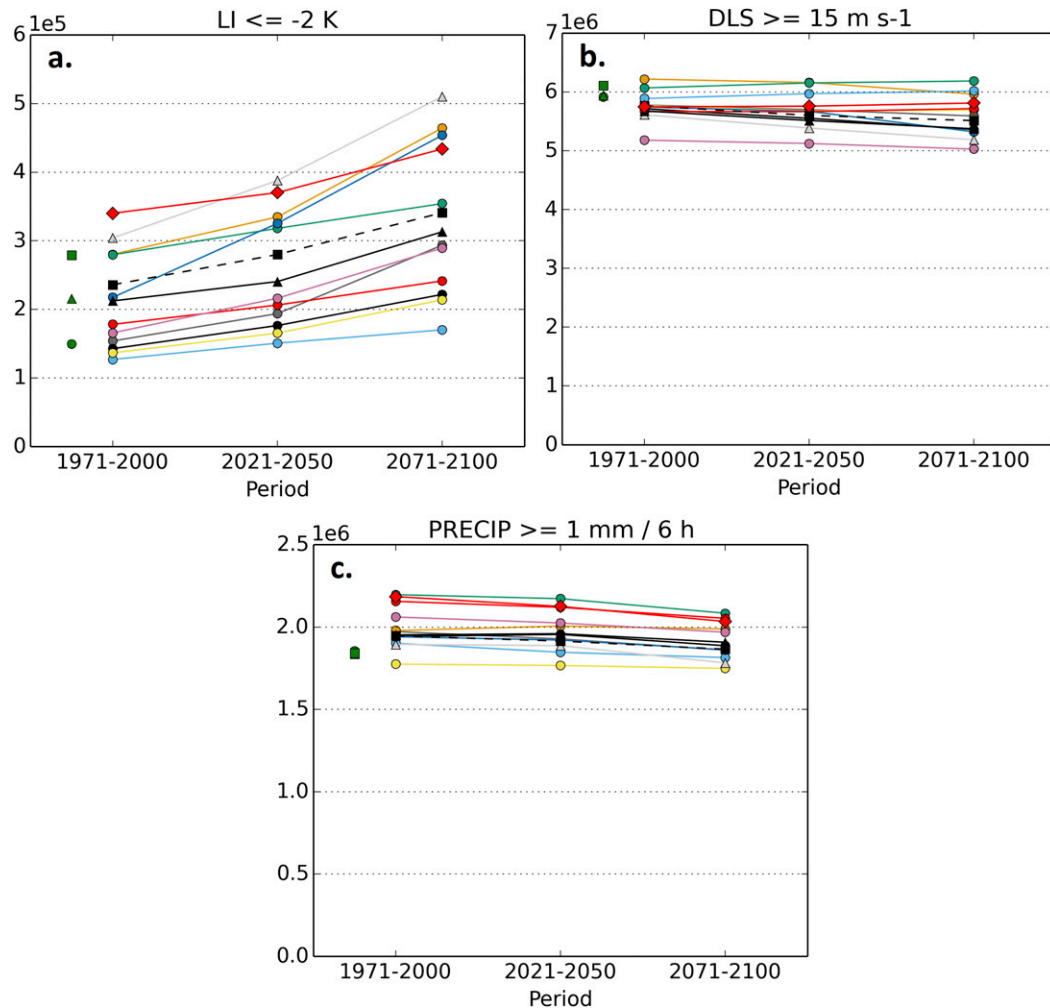


FIG. 16. Mean annual number of (a) unstable, (b) strongly sheared, and (c) precipitating environments in the 1971–2000, 2021–50, and 2071–2100 periods of the RCP8.5 scenario and in the ERA-Interim driven runs (green symbols). The legend for identification of individual models can be found in Fig. 12.

runs suggests that both the regional climate models and the global model drivers are sources of uncertainty. Furthermore, the variability is not equally distributed across Europe. For central and eastern Europe, a robust increase in severe environments frequency was simulated. However, for much of western and southwestern Europe, the found increase was not robust, due to the large ensemble spread. This spread results from the possibility of a reduction of precipitating environments in these areas. Such an effect was also noted in some models for the U.S. Midwest (Diffenbaugh et al. 2013; Seeley and Romps 2015) and for continental Australia (Allen et al. 2014).

An issue we addressed in this study, but did not completely resolve, is that it is unknown how many severe storms develop within an environment with sufficient latent instability and DLS to sustain them. In other

words, it is not known how much of the severe weather potential will actually be used (Trapp et al. 2007a; Diffenbaugh et al. 2013; Seeley and Romps 2015; Tippett et al. 2015). Authors before us have used various approaches to address this issue. For instance, a measure of convective inhibition (CIN) has been used as a proxy for storm initiation by Diffenbaugh et al. (2013) and Gensini and Ashley (2011). Sander (2011) considered CIN as well, while Van Klooster and Roebber (2009) used a neural network approach. For our study, we did not use CIN, because the vertical resolution of data available was not sufficient to compute it. Westermayer et al. (2016) showed that the probability of thunderstorm occurrence increases strongly with increasing midtropospheric relative humidity. We found that future changes in midtropospheric relative humidity in the models (not shown) strongly mimicked the patterns in

the modeled precipitation changes. Here, we addressed the problem of initiation by considering in which simulated unstable and strongly sheared environments models produce precipitation  $\geq 1 \text{ mm (6 h)}^{-1}$ , similar to Trapp et al. (2009). Doing so does not give an estimate of the number of storm events, but it helps to narrow down the strongly sheared and unstable situations to those that are most likely to result in an initiation of (severe) thunderstorms. Naturally, it is not known how accurately the regional climate models produce precipitation where the real atmosphere would and this introduces uncertainty to the projections.

The additional requirement that precipitation must fall makes a difference that is most pronounced across southern and southwestern Europe, where the EURO-CORDEX ensemble simulates a robust decrease in precipitation. This partly compensates for the increase in the instability, yielding less robust changes in the number of (severe) storm environments than in central Europe. Nevertheless, the overall number of unstable and precipitating environments is expected to increase over Europe. This contrasts with the findings of Sander (2011), who found that while CAPE should increase, CIN should do so as well, which would result in fewer, but stronger, convective storms. Trapp and Hoogewind (2016) detected that increases in CIN in simulations of tornado outbreaks under future climate conditions resulted in less widespread storm initiation in some of the convection allowing model simulations. At the same time, increased CAPE resulted in less updraft amplification than would be expected from parcel theory.

The use of high-resolution, convection-allowing models [e.g., by Trapp et al. (2011) or Gensini and Mote (2014, 2015)] may alleviate the problem of studying environmental conditions instead of actual events (Tippett et al. 2015). Convection-permitting simulations prevent the usage of convection parameterization schemes, which have been shown to be a major source of uncertainties in climate change projections (Déqué et al. 2007). However, the fact that Gensini and Mote (2015) note that environmental conditions explain over 80% of the variance associated with modeled severe weather reports provides a lower bound to the accuracy of the approach using environmental conditions across the United States, relative to the use of convection-permitting models. For Europe this number may be different. The resolution of  $0.44^\circ$  used for this study is not sufficient to simulate local maxima or minima in (severe) thunderstorm activity. For example, known maxima of convective hazard occurrence located in the pre-Alpine areas cannot be identified in our simulations, probably because the model is not able to resolve orographically caused mesoscale circulations that modify

the environment around the mountain ranges and modulate latent instability and DLS. Indeed, Prein et al. (2016) showed that enhancing the horizontal grid spacing from  $0.44^\circ$  to  $0.11^\circ$  greatly improves the precipitation simulations in regions with rich orography. Using such higher resolution data would be recommended for future studies.

Another limitation of the present study is that it is limited to severe storms, instead of distinguishing individual hazards. The relationship between severe storm hazards and the large-scale environment is far more complex than can be inferred from latent instability and deep layer shear. For most of the hazards, other factors are important as well, such as the lower tropospheric shear and humidity for tornadoes (Thompson et al. 2003) or the lifted condensation level (Púčik et al. 2015) or freezing level (Dessens et al. 2015) for hail.

Further work is needed to overcome the limitations mentioned above. First, higher-resolution models will be needed to better resolve the topographically induced circulations that affect local severe weather occurrence near mountain ranges. Second, it will be useful to be able to express the trends in occurrence of severe storm environments into event probabilities. This can be done by the development and application of statistical models of the probability of a severe thunderstorm hazard as a function of predictor parameters. In doing so, the individual hazard types can be treated separately, and different trends may result for each hazard. Last, the problems with convective initiation can be alleviated by developing a calibrated statistical model for the probability of storm development as a function of parameters as well.

*Acknowledgments.* We thank the two reviewers, Drs. Victor Gensini and Robert J. Trapp, whose contributions have helped to improve the manuscript. The contributions of Pieter Groenemeijer and Tomáš Púčik to this work were carried out partly within the RAIN project, which has received funding from the European Union's Seventh Framework Programme for research, technological development, and demonstration under Grant Agreement 608166. The contributions of Pieter Groenemeijer and Tomáš Púčik were partly, and those of Anja T. Rädler fully, carried out within the project Analysis of Changes in the Risk of Severe Convective Storms in Europe (ARCS), by Munich Re and the German Ministry of Education and Research (BMBF) under Grant 01LP1525A. The contribution of Tomáš Púčik was carried out partly within MUNI/A/1315/2015 Integrated research of environmental changes in the landscape sphere. The CCLM simulations from the Wegener Center, University of Graz, were

performed at the Jülich Supercomputing Centre (Jülich Supercomputing Centre 2016). The CCLM simulations were supported by the Federal Ministry of Education and Research (BMBF) and performed under the “Konsortial” share at the German Climate Computing Centre (DKRZ). The REMO simulations were supported by CSC (now Climate Service Center Germany, GERICS) and MPIM, as well as BMBF and were performed under the Konsortial share at the German Climate Computing Centre (DKRZ); we are thankful for their various support. The KNMI-RACMO2 simulations were supported by the 7th Framework EU projects IMPACT2C (FP7-ENV.2011.1.1.6-1 Grant 282746) and ECLISE (FP7-ENV.2010.1.1.4-1 Grant 265240), and by the Dutch Ministry of Infrastructure and the Environment. The NUIM WRF simulations were undertaken as part of a project funded by the Irish Environmental Protection Agency. The use of Maynooth University’s high-performance computer and the Irish Centre for High End Computing (ICHEC) Stokes facility is greatly acknowledged.

## APPENDIX

### A List of Used Acronyms and Their Meanings

CanESM2	Second Generation Canadian Earth System Model	NorESM1-M	Norwegian Earth System Model version 1, medium resolution
CCLM4	COSMO Model in Climate Mode, version 4	NUIM	National University of Ireland Maynooth
CNRM-CM5	CNRM-GAME (Météo-France/CNRS) and CERFACS Earth System Model	RACMO22E	Regional Atmospheric Climate Model, version 2 (KNMI)
CSIRO-Mk-3.6.0	Commonwealth Scientific and Industrial Research Organization (Australia) Earth System Model, version 3.6.0	RCA4	Rosby Centre Regional Atmospheric model, version 4
EC-EARTH	European Consortium Earth System Model ( <a href="http://www.ec-earth.org">www.ec-earth.org</a> )	REMO2009	Regional Model of MPI-CSC, 2009 version
GFDL-ESM2M	Geophysical Fluid Dynamics Laboratory–Earth System Model ESM2M	SHMI	Rosby Centre, Swedish Meteorological and Hydrological Institute
HadGEM2-ES	Met Office Hadley Centre Global Environmental Model, version 2	WEGC	Wegener Center for Climate and Global Change, University of Graz, Austria
IPSL-CM5A-MR	Institute Pierre Simon Laplace Coupled Model, version 5A, medium resolution	WRF341	Weather Research and Forecasting Model version 3.41
KNMI	Royal Netherlands Meteorological Institute		
MIROC5	Model for Interdisciplinary Research on Climate of the Center for Climate System Research, The University of Tokyo, Japan		
MPI-CSC	Max Planck Institute–Climate Service Centre		
MPI-ESM-LR	Max Planck Institute–Earth System Model, low resolution		

## REFERENCES

- Allen, J. T., and D. J. Karoly, 2014: A climatology of Australian severe thunderstorm environments 1979–2011: Inter-annual variability and ENSO influence. *Int. J. Climatol.*, **34**, 81–97, doi:[10.1002/joc.3667](https://doi.org/10.1002/joc.3667).
- , —, and K. J. Walsh, 2014: Future Australian severe thunderstorm environments. Part II: The influence of a strongly warming climate on convective environments. *J. Climate*, **27**, 3848–3868, doi:[10.1175/JCLI-D-13-00426.1](https://doi.org/10.1175/JCLI-D-13-00426.1).
- Anderson, G., and D. Klugmann, 2014: A European lightning density analysis using 5 years of ATDnet data. *Nat. Hazards Earth Syst. Sci.*, **14**, 815–829, doi:[10.5194/nhess-14-815-2014](https://doi.org/10.5194/nhess-14-815-2014).
- Brooks, H. E., 2009: Proximity soundings for severe convection for Europe and the United States from reanalysis data. *Atmos. Res.*, **93**, 546–553, doi:[10.1016/j.atmosres.2008.10.005](https://doi.org/10.1016/j.atmosres.2008.10.005).
- , 2013: Severe thunderstorms and climate change. *Atmos. Res.*, **123**, 129–138, doi:[10.1016/j.atmosres.2012.04.002](https://doi.org/10.1016/j.atmosres.2012.04.002).
- , J. W. Lee, and J. P. Craven, 2003: The spatial distribution of severe thunderstorm and tornado environments from global reanalysis data. *Atmos. Res.*, **67–68**, 73–94, doi:[10.1016/S0169-8095\(03\)00045-0](https://doi.org/10.1016/S0169-8095(03)00045-0).
- , A. R. Anderson, K. Riemann, I. Ebberts, and H. Flachs, 2007: Climatological aspects of convective parameters from the NCAR/NCEP reanalysis. *Atmos. Res.*, **83**, 294–305, doi:[10.1016/j.atmosres.2005.08.005](https://doi.org/10.1016/j.atmosres.2005.08.005).
- Craven, J. P., R. E. Jewell, and H. E. Brooks, 2002: Comparison between observed convective cloud-base heights and lifting condensation level for two different lifted parcels. *Wea. Forecasting*, **17**, 885–890, doi:[10.1175/1520-0434\(2002\)017<0885:CBOCCB>2.0.CO;2](https://doi.org/10.1175/1520-0434(2002)017<0885:CBOCCB>2.0.CO;2).
- Dee, D. P., and Coauthors, 2011: The ERA-Interim reanalysis: Configuration and performance of the data assimilation system. *Quart. J. Roy. Meteor. Soc.*, **137**, 553–597, doi:[10.1002/qj.828](https://doi.org/10.1002/qj.828).
- Del Genio, A. D., M.-S. Yao, and J. Jonas, 2007: Will moist convection be stronger in a warmer climate? *Geophys. Res. Lett.*, **34**, L16703, doi:[10.1029/2007GL030525](https://doi.org/10.1029/2007GL030525).
- Déqué, M., and Coauthors, 2007: An intercomparison of regional climate simulations for Europe: Assessing uncertainties in model projections. *Climatic Change*, **81** (Suppl. 1), 53–70, doi:[10.1007/s10584-006-9228-x](https://doi.org/10.1007/s10584-006-9228-x).

- Dessens, J., C. Berthet, and J. L. Sanchez, 2015: Change in hailstone size distributions with an increase in the melting level height. *Atmos. Res.*, 158–159, 245–253, doi:10.1016/j.atmosres.2014.07.004.
- Diffenbaugh, N. S., M. Scherer, and R. J. Trapp, 2013: Robust increases in severe thunderstorm environments in response to greenhouse forcing. *Proc. Natl. Acad. Sci. USA*, **110**, 16 361–16 366, doi:10.1073/pnas.1307758110.
- Doswell, C. A., III, and E. N. Rasmussen, 1994: The effect of neglecting the virtual temperature correction on CAPE calculations. *Wea. Forecasting*, **9**, 625–629, doi:10.1175/1520-0434(1994)009<0625:TEONTV>2.0.CO;2.
- , H. E. Brooks, and R. A. Maddox, 1996: Flash flood forecasting: An ingredients-based methodology. *Wea. Forecasting*, **11**, 560–581, doi:10.1175/1520-0434(1996)011<0560:FFFAIB>2.0.CO;2.
- Dotzek, N., P. Groenemeijer, B. Feuerstein, and A. M. Holzer, 2009: Overview of ESSL's severe convective storms research using the European Severe Weather Database ESWD. *Atmos. Res.*, **93**, 575–586, doi:10.1016/j.atmosres.2008.10.020.
- Duda, J. D., and W. A. Gallus Jr., 2010: Spring and summer Midwestern severe weather reports in supercells compared to other morphologies. *Wea. Forecasting*, **25**, 190–206, doi:10.1175/2009WAF2222338.1.
- Galway, J. G., 1956: The lifted index as a predictor of latent instability. *Bull. Amer. Meteor. Soc.*, **37**, 528–529.
- Gensini, V. A., and W. S. Ashley, 2011: Climatology of potentially severe convective environments from North American regional reanalysis. *Electron. J. Severe Storms Meteor.*, **6** (8). [Available online at <http://www.ejssm.org/ojs/index.php/ejssm/article/viewArticle/85>.]
- , and T. L. Mote, 2014: Estimations of hazardous convective weather in the United States using dynamical downscaling. *J. Climate*, **27**, 6581–6589, doi:10.1175/JCLI-D-13-00777.1.
- , and —, 2015: Downscaled estimates of late 21st century severe weather from CCSM3. *Climatic Change*, **129**, 307–321, doi:10.1007/s10584-014-1320-z.
- , C. A. Ramseier, and T. L. Mote, 2014: Future convective environments using NARCCAP. *Int. J. Climatol.*, **34**, 1699–1705, doi:10.1002/joc.3769.
- Giorgi, F., C. Jones, and G. R. Asrar, 2009: Addressing climate information needs at the regional level: The CORDEX framework. *WMO Bull.*, **58**, 175–183.
- Groenemeijer, P. H., and A. van Delden, 2007: Sounding-derived parameters associated with large hail and tornadoes in the Netherlands. *Atmos. Res.*, **83**, 473–487, doi:10.1016/j.atmosres.2005.08.006.
- , and T. Kühne, 2014: A climatology of tornadoes in Europe: Results from the European Severe Weather Database. *Mon. Wea. Rev.*, **142**, 4775–4790, doi:10.1175/MWR-D-14-00107.1.
- Jacob, D., and Coauthors, 2014: EURO-CORDEX: New high-resolution climate change projections for European impact research. *Reg. Environ. Change*, **14**, 563–578, doi:10.1007/s10113-013-0499-2.
- Johns, R. H., and C. A. Doswell III, 1992: Severe local storms forecasting. *Wea. Forecasting*, **7**, 588–612, doi:10.1175/1520-0434(1992)007<0588:SLSF>2.0.CO;2.
- Jülich Supercomputing Centre, 2016: JURECA: General-purpose supercomputer at Jülich Supercomputing Centre. *J. Large-Scale Res. Facil.*, **2**, A62, doi:10.17815/jlsrf-2-121.
- Kapsch, M. L., M. Kunz, R. Vitolo, and T. Economou, 2012: Long-term trends of hail-related weather types in an ensemble of regional climate models using a Bayesian approach. *J. Geophys. Res.*, **117**, D15107, doi:10.1029/2011JD017185.
- Kotlarski, S. K., and Coauthors, 2014: Regional climate modeling on European scales: A joint standard evaluation of the EURO-CORDEX RCM ensemble. *Geosci. Model Dev.*, **7**, 1297–1333, doi:10.5194/gmd-7-1297-2014.
- Kunz, M., 2007: The skill of convective parameters and indices to predict isolated and severe thunderstorms. *Nat. Hazards Earth Syst. Sci.*, **7**, 327–342, doi:10.5194/nhess-7-327-2007.
- Marsh, P. T., H. E. Brooks, and D. J. Karoly, 2009: Preliminary investigation into the severe thunderstorm environment of Europe simulated by the Community Climate System Model 3. *Atmos. Res.*, **93**, 607–618, doi:10.1016/j.atmosres.2008.09.014.
- Mohr, S., M. Kunz, and K. Keuler, 2015: Development and application of a logistic model to estimate the past and future hail potential in Germany. *J. Geophys. Res. Atmos.*, **120**, 3939–3956, doi:10.1002/2014JD022959.
- Moss, R. H., and Coauthors, 2010: The next generation of scenarios for climate change research and assessment. *Nature*, **463**, 747–756, doi:10.1038/nature08823.
- Normand, C. W. B., 1938: On instability from water vapour. *Quart. J. Roy. Meteor. Soc.*, **64**, 47–70, doi:10.1002/qj.49706427306.
- Poelman, D. R., W. Schulz, G. Diendorfer, and M. Bernardi, 2016: The European lightning location system EUCLID—Part 2: Observations. *Nat. Hazards Earth Syst. Sci.*, **16**, 607–616, doi:10.5194/nhess-16-607-2016.
- Prein, A. F., G. J. Holland, R. M. Rasmussen, J. Done, K. Ikeda, M. P. Clark, and C. H. Liu, 2013: Importance of regional climate model grid spacing for the simulation of heavy precipitation in the Colorado headwaters. *J. Climate*, **26**, 4848–4857, doi:10.1175/JCLI-D-12-00727.1.
- , and Coauthors, 2015: A review on regional convection-permitting climate modeling: Demonstrations, prospects, and challenges. *Rev. Geophys.*, **53**, 323–361, doi:10.1002/2014RG000475.
- , and Coauthors, 2016: Precipitation in the EURO-CORDEX 0.11° and 0.44° simulations: High resolution, high benefits? *Climate Dyn.*, **46**, 383–412, doi:10.1007/s00382-015-2589-y.
- Púčik, T., P. Groenemeijer, D. Rýva, and M. Kolář, 2015: Proximity soundings of severe and nonsevere thunderstorms in central Europe. *Mon. Wea. Rev.*, **143**, 4805–4821, doi:10.1175/MWR-D-15-0104.1.
- Rasmussen, E. N., and D. O. Blanchard, 1998: A baseline climatology of sounding-derived supercell and tornado forecast parameters. *Wea. Forecasting*, **13**, 1148–1164, doi:10.1175/1520-0434(1998)013<1148:ABCOSD>2.0.CO;2.
- Sander, J., 2011: Extremwetterereignisse im Klimawandel: Bewertung der derzeitigen und zukünftigen Gefährdung. Ph.D. thesis, University of Munich, 125 pp.
- Schulz, W., G. Diendorfer, S. Pedebay, and D. R. Poelman, 2016: The European lightning location system EUCLID—Part 1: Performance analysis and validation. *Nat. Hazards Earth Syst. Sci.*, **16**, 595–605, doi:10.5194/nhess-16-595-2016.
- Seeley, J. T., and D. M. Romps, 2015: The effect of global warming on severe thunderstorms in the United States. *J. Climate*, **28**, 2443–2458, doi:10.1175/JCLI-D-14-00382.1.
- Taylor, K. E., R. J. Stouffer, and G. A. Meehl, 2012: An overview of CMIP5 and the experiment design. *Bull. Amer. Meteor. Soc.*, **93**, 485–498, doi:10.1175/BAMS-D-11-00094.1.
- Thompson, R. L., R. Edwards, J. A. Hart, K. L. Elmore, and P. Markowski, 2003: Close proximity soundings within supercell environments obtained from the Rapid Update Cycle. *Wea. Forecasting*, **18**, 1243–1261, doi:10.1175/1520-0434(2003)018<1243:CPSWSE>2.0.CO;2.

- Tippett, M. K., J. T. Allen, V. A. Gensini, and H. E. Brooks, 2015: Climate and hazardous convective weather. *Curr. Climate Change Rep.*, **1**, 60–73, doi:[10.1007/s40641-015-0006-6](https://doi.org/10.1007/s40641-015-0006-6).
- Trapp, R. J., and K. A. Hoogewind, 2016: The realization of extreme tornadic storms events under future anthropogenic climate change. *J. Climate*, **29**, 5251–5265, doi:[10.1175/JCLI-D-15-0623.1](https://doi.org/10.1175/JCLI-D-15-0623.1).
- , B. A. Halvorson, and N. S. Diffenbaugh, 2007a: Telescoping, multimodel approaches to evaluate extreme convective weather under future climates. *J. Geophys. Res.*, **112**, D20109, doi:[10.1029/2006JD008345](https://doi.org/10.1029/2006JD008345).
- , N. S. Diffenbaugh, H. E. Brooks, M. E. Baldwin, E. D. Robinson, and J. S. Pal, 2007b: Changes in severe thunderstorm environment frequency during the 21st century caused by anthropogenically enhanced global radiative forcing. *Proc. Natl. Acad. Sci. USA*, **104**, 19 719–19 723, doi:[10.1073/pnas.0705494104](https://doi.org/10.1073/pnas.0705494104).
- , —, and A. Gluhovsky, 2009: Transient response of severe thunderstorm forcing to elevated greenhouse gas concentrations. *Geophys. Res. Lett.*, **36**, L01703, doi:[10.1029/2008GL036203](https://doi.org/10.1029/2008GL036203).
- , E. D. Robinson, M. E. Baldwin, N. S. Diffenbaugh, and B. R. Schwedler, 2011: Regional climate of hazardous convective weather through high-resolution dynamical downscaling. *Climate Dyn.*, **37**, 677–688, doi:[10.1007/s00382-010-0826-y](https://doi.org/10.1007/s00382-010-0826-y).
- Van Klooster, S. L., and P. J. Roebber, 2009: Surface-based convective potential in the contiguous United States in a business-as-usual future climate. *J. Climate*, **22**, 3317–3330, doi:[10.1175/2009JCLI2697.1](https://doi.org/10.1175/2009JCLI2697.1).
- Weisman, M. L., and J. B. Klemp, 1982: The dependence of numerically simulated convective storms on vertical wind shear and buoyancy. *Mon. Wea. Rev.*, **110**, 504–520, doi:[10.1175/1520-0493\(1982\)110<0504:TDONSC>2.0.CO;2](https://doi.org/10.1175/1520-0493(1982)110<0504:TDONSC>2.0.CO;2).
- , W. C. Skamarock, and J. B. Klemp, 1997: The resolution dependence of explicitly modeled convective systems. *Mon. Wea. Rev.*, **125**, 527–548, doi:[10.1175/1520-0493\(1997\)125<0527:TRDOEM>2.0.CO;2](https://doi.org/10.1175/1520-0493(1997)125<0527:TRDOEM>2.0.CO;2).
- Westermayer, A. T., P. Groenemeijer, G. Pistotnik, R. Sausen, and E. Faust, 2016: Identification of favorable environments for thunderstorms in reanalysis data. *Meteor. Z.*, **26**, 59–70, doi:[10.1127/metz/2016/0754](https://doi.org/10.1127/metz/2016/0754).